RADIOACTIVE AU FOR POTENTIAL RADIOTHERAPEUTIC APPLICATION

A Thesis

presented to

the Faculty of the Graduate School

at the University of Missouri

In Partial Fulfillment

of the Requirements for the Degree

Master of Arts

---

by

PARA KAN

Silvia S. Jurisson, Ph.D., Thesis Supervisor

Cathy S. Cutler, Ph.D., Co-Advisor

JULY 2010

The undersigned, appointed by the Dean of the Graduate School, have examined the thesis entitled

RADIOACTIVE AU FOR POTENTIAL
RADIOTHERAPEUTIC APPLICATIONS

Presented by Para Kan

A candidate for the degree of Master of Science

And hereby certify that in their opinion it is worthy of acceptance.

_____
Silvia S. Jurisson, Ph.D.

_____
Cathy S. Cutler, Ph.D.

_____
Timothy Hoffman, Ph.D.

DEDICATION

I would like to thank God for looking over me throughout my life and blessing me with a tremendous amount of support especially during rough times. I will always be in debt to my church, The First Lutheran Church of South Bend, WA, who sponsored my family from a Cambodian concentration camp in Thailand during the civil war in Cambodia.

This thesis is dedicated to in loving memory of Marie E. Noren and her husband, Harry Noren. Both have greatly assisted my family with their transition to a new world, the United States of America.

I owe my community of South Bend, WA, my thanks for raising me right and providing me with the opportunity to learn and be a contributing citizen to society. I would also like to thank Andrew & Virginia Carlson for their guidance and support throughout my high school years. It has laid the foundation to who I am today.

Finally, I would like to thank my family, Bun Kray Kan (Mom), Vong Kan (Dad), Sara Kan (Sister), and "Sally" Huaqiong Sun (Wife). You mean so much to me and thanks for all that you have done.

ACKNOWLEDGMENTS

I would like to thank my advisors, Silvia S. Jurisson, Ph.D. and Cathy S. Cutler, Ph.D. for their continued support throughout my graduate career at the University of Missouri. I would also like to thank the University of Missouri Chemistry Dept., the Electron Microscopy Center, the Nuclear Engineering and Science Institute (NSEI), Radiology, and the University of Missouri Research Reactor (MURR) for the use of their facilities for conducting my research.

The funding for my research was made possible by the Graduate Assistant for Areas of National Need (GAANN) Grant from Sudarshan K. Loyalka, Ph.D., NSEI and the National Cancer Institute (NCI) Grant from Kattesh V. Katti, Ph.D., Radiology.

Table of Contents

LIST OF TABLES AND FIGURES

LIST OF TABLES AND FIGURES (CONT.)

RADIOACTIVE AU FOR POTENTIAL RADIOTHERAPEUTIC APPLICATIONS

Para Kan

Silvia S. Jurisson, Ph.D., Thesis Supervisor

Cathy S. Cutler, Ph.D., Co-Advisor

ABSTRACT

Radioactive gold-198/199 can be used in therapeutic radiopharmaceutical agents to combat cancer. In this thesis, two projects involving the development of radioactive gold-198/199 are described. The first project discusses the first tetradentate Au(III) bis-thiosemicarbazones (Au-ATSM/PTSM) that were synthesized and characterized. At radiotracer levels using Au-198/199 required a high ratio of gold-to-ligand (1:>100). Our studies indicated that Au(III) can be coordinated to both ATSM or PTSM ligands. These results allowed for further investigation into a variety of bis-thiosemicarbazide derivatives to coordinate Au(III).

The second project involved radioactive gold nanoparticles (AuNPs) that were synthesized, characterized, and evaluated *in vivo*. Three stabilizing agents (starch, gum Arabic, and epigallocatechin gallate) were studied to determine the ease of syntheses of AuNPs, relative stability to aggregation, and toxicity *in vivo*. Incorporating radioactive Au-198/199 allowed for biodistribution studies by three administration routes (intravenous, intraperitoneal, and intratumoral injections) in prostate cancer bearing mice. These studies indicated that radioactive (Au-198/199) AuNPs can be used to treat prostate cancer by intratumoral injection. Two of the three stabilizers (starch and epigallocatechin gallate) were further evaluated for treating prostate tumors in mice. The

results indicated that the radioactive AuNPs reduced the tumor size with no apparent toxic effects.

Chapter 1: Introduction

1.1 Radiation and Nuclear Medicine:

Radiation is a part of everyday life. Our bodies, whether inside our homes or offices, or outside during a hot sunny day or a cool evening night, are constantly exposed to radiation. Too much radiation can increase risks for certain types of cancer. Too little radiation can be harmful as well. Plants need a certain amount of ultraviolet (UV) light to assist in photosynthesis. If there is no UV light present for these plants, certain chemical reactions within plants cannot occur[1]. Also, X-rays in low doses can have a stimulating effect on plant growth[2]. Low levels of X-ray exposure to seeds and roots have been shown to increase the size of the overall plant, with no abnormal deformity[3, 4].

Although not much is understood on how low-level radiation exposure to gamma-rays affects plants and animals, high-level exposures can cause cell mutations and cell damage, particularly during cell replication[5]. In nuclear medicine, gamma-rays are used to provide physiological images to locate tumors within the body. The dose that the patient receives from a nuclear medicine image procedure has no side-effects. This is because the dose is not high enough to produce radiation induced damage to cells and tissue. For therapy, a radioisotope emitting alphas, betas, or Aüger electrons is used. Finding the right radioisotope with the appropriate nuclear properties for nuclear medicine applications requires attention to how the compound is made, what the emission properties are, and the half-life. In this thesis, the focus will be on Au(III) and Au(0) chemistry and its applications as potential radiopharmaceutical agents.

1.2. Gold in Medicine

Medicinal applications for gold have been practiced by ancient cultures such as those from Egypt, India, and China[6]. Gold was used to treat some diseases such as smallpox, skin ulcers, syphilis, and measles[6]. In the second chapter, the use of Au(III) is discussed along with two bifunctional chelates that were used to stabilize Au(III) from reduction. Bifunctional chelates coordinate radioactive atoms and connect to a linker that is usually bound to a targeting moiety (i.e., antibody or peptide). The bifunctional chelates that were used were bis-thiosemicarbazides. Both, Au(III) complexes and bis-thiosemicarbazides, are known for their anti-tumor properties[6-8]. By combining the two, this could increase the effectiveness of a drug against tumor growth. Incorporating radioactive Au-198/199 might then allow for detecting the compound and determining where the drug will localize and how it will be excreted *in vivo*. Radioactive Au-198/199 are both gamma- and beta-emitters.

Gold drugs have been widely used in treating symptoms of rheumatoid arthritis. Three of the most common gold drugs for treating the pain and stiffness are sodium aurothiomalate (Myochrisin), aurothioglucose (Solganol), and auranofin (Riduara)[6]. Aurothiomalate and aurothioglucose are oligomers that require administration via intramuscular injection every week[6]. These gold compounds are rapidly absorbed, then cleared throughout various organs including the kidneys and liver[9]. Toxicity in the kidneys and liver are common along with mouth ulcers, skin reactions, and blood disorders[9]. In an effort to reduce toxicity and improve pharmacokinetics, auranofin was

introduced in 1979[10], then later approved in 1985[6]. Auranofin was the first gold drug administered orally[10]. Toxicity was reduced because there was less retention of gold in the tissues and renal toxicity dropped significantly[9, 10]. The mechanism of auranofin is not completely known, but it has been suggested that auranofin is metabolized within the cells and inhibits superoxides or hydroxyl radicals[6, 9]. The gold reacts with the cyanide that is released during the phagocytosis (removal of dead or foreign cells) of the immune system allowing this newly formed gold compound, aurocyanide ($AuCN_2^-$), to easily enter cells to inhibit oxidative reactions[6, 9, 10].

Gold has also been examined as an anti-malarial agent. Several strains of malaria have been known to be resistant to choloroquine and sulfadoxine-pyrimethamine, two common and inexpensive drugs[11]. One drug resistant strain of malaria, *plasmodium falciparum,* is known to be sensitive to oxidative stress[10]. Researchers have found that combining artemisinin (a drug commonly used to treat malaria) with auranofin provides a very potent drug against malaria. *In vitro,* only nanomolar quantities were required to inhibit 50% of the growth of *plasmodium falciparum*[10]. As harmful bacteria evolves and becomes drug resistant so to must the medication that is designed to treat them.

1.3. Gold Nanoparticles

Recently most work pertaining to Au centers around Au nanoparticles (AuNPs)[12], which are colloidal particles that ranges from 1 to several hundred nanometers in size. Gold(0) is thermodynamically more stable than Au(III). This metal is most known for its application in jewelry because of its luster and inertness. In fact, gold is so stable in the

metallic form that converting gold metal to Au(III) requires the use of hot aqua regia. It is this property that makes gold an attractive element for producing nanosize colloids. Generally, Au(III) can be readily reduced by any mild reducing agent. The process is usually very rapid (less than a few hours) and the shelf-life of these AuNPs is fairly long (at least a few months). Rapid syntheses and stability are important for developing a radiopharmaceutical agent. Another attractive characteristic of AuNPs is the ability to modify its surface. All AuNPs require stabilizers that provide a protective layer preventing large aggregates. If no stabilizers are present, then Au-Au interactions cause formation of gold macro-particles that can be visible to the naked eye. Modifications can be made on the stabilizers to allow for functionality depending on the application. For cancer therapy, attaching a targeting moiety will allow for affinity for receptor sites.

Industries provide AuNPs labeled with IgB antibodies (AuroProbe) for immunodetection on membranes[13]. Since Au is a high Z metal, this increases the contrast image under electron microscopy. The future direction of AuNPs appears to be in drug delivery as more companies are allocating resources to make these nanomatericals multifunctional and controllable by external signals[14]. One example includes the use of placing non-radioactive AuNPs within a tumor then targeting the tumor with an x-ray beam. The energy from the x-rays is absorbed by Au and increases the CT (computed tomography) image. Gold metal has K-edge at 80.7 keV and exhibits a higher absorption for X-rays than iodine (K-edge 33 keV) thus, minimizing bone and tissue interference achieving a higher contrast with lower X-ray dose. Iodinated agents are non-specific and clear the blood stream faster than the time required to image certain organs. Gold

nanoparticles are target specific and are eliminated from the blood more slowly than iodine agents, permitting optimum imaging times[15]. Another use would be for treatment, where a high concentration of AuNPs was implanted in the tumor. The x-ray beam would be concentrated on the location of the AuNPs causing the Au atoms to become excited. Upon relaxation, these Au atoms release heat destroying nearby cells.

1.4. Gold (III) Chemistry

Gold (III) compounds are predominately square planar and have a diamagnetic, d^8 outer electron shell configuration. Gold (III) has an ionic radius of 0.85 Å, much smaller than gold (I) of 1.37 Å. Coordination to Au(III) usually involves oxygen, nitrogen, halide, cyanide, azide, isocyanide, phosphorus, and sulfur[16].

1.5. Radiotherapy Using Au-198 and Au-199

For radiopharmaceutical applications, the type of emission of a radioisotope is important. For treatment, radioisotopes that emit particles such as betas, alphas, and Aüger electrons can be used. These emitted particles can cause multiple single-strand or double-strand breaks within the helices of DNA, thus preventing cell replication. Both Au-198 and Au-199 are beta and gamma emitters. The gammas emitted allow for detection of the radioactive gold *in vivo*. Incorporating a high enough dose will provide enough activity to destroy tumors.

Current radiotherapy involving Au-198 includes using Au-198 colloid in treating carcinoma of the prostate[17], cervix uteri[17], and liver[18]. Gold-198 seeds or wires are also

used in interstitial implantation in tumors[17]. Gold-198 colloid is also used for imaging the liver. Health insurers approve of brachytherapy (also known as interstitial radiation, intracavitary radiation, internal radiation therapy) for the treatment of cancer.

In this thesis, Au(III) bis-thiosemicarbazones (Chapter 2) and AuNPs (Chapters 3 and 4) are studied. Each Au compound was synthesized and evaluated for radiopharmaceutical applications.

Chapter 2: Synthesis and Characterization of Gold (III) Bis-thiosemicarbazones: Au-ATSM and Au-PTSM

2.1 Introduction

The nuclear properties of Au-199 are ideal for radiopharmaceutical applications. Gold-199 is a beta and gamma emitter with a maximum beta energy of 0.46 MeV and two imagable gamma photons at 158 and 208 keV, with a half-life of 3.14 days that allows sufficient time for producing, shipping, and administering a Au-199 radiolabeled drug.

Gold-199 can be produced with high specific activity, where ~100% of the Au atoms are Au-199. The production of Au-199 can be made from a single neutron capture of Pt-198 to form Pt-199. Pt-199 has a half-life of 30.2 min and emits a beta particle and gamma ray to decay to Au-199. The chemical difference between the two elements allows for separation and higher specific activity.

An alternative, direct method of producing Au-199 is from a double neutron capture of natural, monoisotopic Au-197. Both Au-197 and Au-198 have large nuclear cross-sections allowing for a high probability of capturing a thermal or epithermal neutron. Though the specific activity is greatly reduced from this production approach, this is a faster and simpler method to produce radioactive Au. For radiopharmaceutical development, optimizing reaction conditions using Au-198 is preferred because this can allow for macroscopic syntheses, which provide easier characterization than using Au-199. Gold is commonly used in jewelry applications and is a valuable commodity due to its rarity and stability to oxidation. Au(III) complexes are generally susceptible to

reduction to Au(0)[19]. Au(III) compounds and bis-thiosemicarbazides have both been known for their anti-tumor properties[7]. By combining Au(III) and bis-thiosemicarbazide ligands, this could increase the pharmacological effect. The ligands that were investigated for Au(III) complexation are ATSM (diacetyl thiosemicarbazide) and PTSM (pyruvic thiosemicarbazide). Both ligands are tetradentate with two imine nitrogen and two thiolate sulfur donor atoms. This will be the first reported tetradentate bis-thiosemicarbazone that coordinates with Au(III).

The Au(III) complexes presented in this chapter are Au-ATSM and Au-PTSM. An X-ray crystallographic structure of [Au-ATSM]$AuCl_4 \bullet$ 2MeOH was obtained indicating that the square plane around the Au(III) center is somewhat strained (Table 2-2). NMR and ESI-MS data were obtained for both Au-ATSM and Au-PTSM confirming their structures. Other reported Au(III) tetradentate compounds also show a strained square plane around Au(III)[7].

2.2. Experimental Section

2.2.1 General

Gold metal, $NaAuCl_4 \cdot 2H_2O$, pyruvic aldehyde (40% w/w), 2,3-butanedione (diacetyl), N^4-methyl-thiosemicarbazide, N^4-ethyl-thiosemicarbazide, methanol and dichloromethane were purchased from Alfa Aesar and used without further purification. Absolute ethanol was manufactured by Aaper Alcohol and Chemical Co. All water used was 18 MΩ. Whatman Cellulose thin-layer chromatography (TLC) plates were purchased from Sigma-Aldrich. All solvents and acids were reagent grade and purchased

from Fisher Scientific and used without further purification. ^{198}Au was prepared by the University of Missouri Research Reactor Center using an (n,γ) reaction on natural gold foil. A 0.08-mg sample of Au foil was irradiated in a reflector position in the reactor at a thermal neutron flux of 8.72×10^{13} n cm^{-2} s^{-1}.

Plexiglass and lead shielding were used when working with ^{198}Au. Radiation safety procedures were followed at all times by trained personnel in radiation-approved laboratories. Animal studies were performed under procedures approved by the Animal Care and Use Committee at the Harry S Truman VA Hospital.

2.2.2. Physical measurements

^{1}H and ^{13}C NMR spectra were obtained in d_6-DMSO or d_3-CD_3CN on a Bruker ARX-300 spectrometer. Electrospray ionization mass spectra were obtained on a Thermo Finnigan TSQ7000 triple-quadrupole instrument with an API2 source at the University of Missouri. Elemental analyses were performed by Quantitative Technologies Inc. (QTI; Whitehouse, NJ). A Bioscan 200 TLC scanner was used to count radioactivity of TLC plates and paper chromatographs from ^{198}Au experiments. A NaI(Tl) well counter was used to assay ^{198}Au liquid samples.

2.2.3. Thiosemicarbazone ligands

The thiosemicarbazone ligands were prepared as previously reported [8, 20]. Briefly, one equivalent of the appropriate diketone was added dropwise to 2 equivalents of the appropriate thiosemicarbazide in 5% acetic acid and heated to 60–65°C for 4 h. On

cooling, the crude product precipitated. The product was recrystallized from a boiling ethanol/water (50:50) solution and dried under vacuum. NMR spectra were taken in d_6-DMSO and were consistent with literature values.

2.2.4. [Au(ATSM)]$AuCl_4$

$NaAuCl_4 \cdot 2H_2O$ (0.139 g; 0.3 mmol) was dissolved in 3 ml of ethanol. Diacetyl-bis(N^4-methylthiosemicarbazone) (ATSM; 0.088g; 0.35 mmol) was sonicated in 3 ml of ethanol for 30 min. The two solutions were then combined and allowed to stir for several min until an intense dark purple color was observed. The resultant solution was cooled and red crystals were collected by filtration, washed with diethyl ether and dried in vacuo for 2 days (yield 14.9% based on complex; 29.8% based on Au). Recrystallization from methanol with toluene vapor diffusion yielded X-ray-quality crystals. ESI/APCI mass spectrum: M^+ at 455.00 (455.33 calcd). ^{1}H-NMR (DMSO-d_6): 2.30 ppm (s, 6H, C*H*3C=N), 3.06 ppm (s, 6H, CH_3NH), 7.65 ppm (b, 2H, N*H*CH_3), 9.39 ppm (s, 2H, NN*H*CS). Anal. Calc'd (found) for $Au_2C_8H_{14}N_6S_2Cl_4 \cdot 0.75$ EtOH: C, 15.55 (15.21); H, 2.55 (2.7); N, 9.89 (10.9); S, 7.55 (7.51).

2.2.5. [Au(PTSM)]$AuCl_4$

This compound was synthesized as described above for [Au(ATSM)]$AuCl_4$, substituting the equivalent molar quantity of PTSM for ATSM. The dark purple precipitate was collected, washed with diethyl ether and dried in vacuo for 2 days yielding the final product (yield 18.4% based on complex; 36.8% based on Au).

ESI/APCI mass spectrum: M^+ at 441.02 (441.39 calcd). ^{1}H NMR (d_6-DMSO): 2.17 ppm (s, 3H, CC*H*$_3$), 2.71 ppm (s, 3H, NHC*H*$_3$), 3.01 (s, 3H, NHC*H*$_3$), 8.20 (s, H, N=C*H*), 9.38 ppm, (b, H, CN*H*CH$_3$), 9.61 ppm (b, H, CN*H*CH$_3$). Anal. Calc'd (found) for $Au_2C_7H_{12}N_6S_2Cl_4$: C, 10.78 (10.6); H, 1.55 (1.54); N, 10.77 (10.18); S, 8.22 (9.72).

2.2.6. X-ray Structure Determinations and Refinements for [Au(ATSM)]AuCl$_4$·2MeOH

Intensity data were obtained at −100°C on a Bruker SMART CCD Area Detector system using the ω scan technique with Mo Kα radiation from a graphite monochromator. Intensities were corrected for Lorentz and polarization effects. Equivalent reflections were merged, and absorption corrections were made using the multiscan method. Space groups, lattice parameters and other relevant information are given in Table 2-1. The structures were solved by direct methods with full-matrix least-squares refinement, using the SHELX package[21, 22]. All non-hydrogen atoms were refined with anisotropic thermal parameters. The hydrogen atoms, except those of the waters of crystallization, were placed at calculated positions and included in the refinement using a riding model, with fixed isotropic *U*. Data were corrected for decay and absorption using the program SADABS[23]. The final difference maps contained no features of chemical significance.

2.2.7. [Au-198] Au-ATSM and Au-PTSM Synthesis (radiotracer)

Two methods were used to synthesize ^{198}Au-PTSM and ^{198}Au-ATSM.

Method 1: The solid ligands (ATSM or PTSM) were loaded onto a 9-cm Bio-Rad® poly-prep column with 0.45 μm nylon syringe filter. 2 mL of TBA-$^{198}AuCl_4$ (tetrabutylammonium tetrachloroaurate) in ethanol or 2 mL of $H^{198}AuCl_4$ in 0.5 or 3 M HCl was then added to the column. An immediate purple color could be observed from the instantaneous reaction to form ^{198}Au-PTSM and ^{198}Au-ATSM. A syringe was used to pump air through the column to force the elution of the ^{198}Au complex. The column was washed with 2 mL of ethanol at least 3 times to elute ^{198}Au-PTSM and ^{198}Au-ATSM.

Method 2: The ligand was sonicated in pure ethanol for at least 20 min. (The ligand did not fully dissolve.) This mixture was then added to a solution of TBA-$^{198}AuCl_4$ or $H^{198}AuCl_4$ in ethanol. An instant color change from yellow to dark purple was observed. The reaction mixture was allowed to react for 10 to 20 min, and was then filtered through glass wool. The Au(III) complex was filtered again using a 0.45 μm nylon syringe filter.

Each method was analyzed by radiochromatography to determine the percentage of TBA-$^{198}AuCl_4$, $H^{198}AuCl_4$, [^{198}Au-ATSM], (or [^{198}Au-PTSM]), and ^{198}Au colloid that were present.

2.2.8. [Au-199] Synthesis of Au-ATSM and Au-PTSM

Natural Pt foil (7 mg) was irradiated for 30 min in a pneumatic tube at MURR. The irradiated foil was dissolved in 2 mL of hot aqua regia. The solution was taken to near dryness followed by a 2 mL addition of 3 M HCl. The HCl was heated to near dryness again. Next, 1 mL of 3 M HCl was added and the solution was cooled to room

temperature. The solution of radioactive H_2PtCl_6 was transferred to a centrifuge vial with an equal volume of ethyl acetate added to the vial and vortexed. The $H^{199}AuCl_4$ extracts into the ethyl acetate, while the H_2PtCl_6 remains in the lower aqueous layer. The upper organic layer was collected to isolate the carrier-free $H^{199}AuCl_4$.

To the $H^{199}AuCl_4$ solution, 2 mL of 0.1 M TBA-Cl in chloroform was added and thoroughly mixed to make TBA-$^{199}AuCl_4$. The chloroform and ethyl acetate was dried using a steady airflow. One mL of ethanol was then added and vortexed. The activity of ^{199}Au was 37.5 μCi. ATSM (6 mg) was fully dissolved in 1 mL of DMSO. TBA-$^{199}AuCl_4$ (100 μL) and ATSM (100 μL) solutions were combined and vortexed. The reaction yield was characterized using radiochromatography with cellulose TLC plates developed in methanol with HCl.

2.2.9. In-Vitro Stability

In-Vitro assays were conducted with rat serum, PBS (phosphate buffered saline), and saline solutions. These solutions were incubated in a 37^{o}C water bath. Purified ^{198}Au-ATSM (100 μL) was added to each one mL solution and then a 10-μL aliquot was analyzed by radiochromatography at the following time points: 15 min, 1 h, 4 h, and 24 h.

2.3. Results and Discussion

[Au-ATSM]$AuCl_4$ and [Au-PTSM]$AuCl_4$ are the first Au(III) tetradentate bis-thiosemicarbazone compounds reported. A few groups have reported tri- and bidentate Au(III) thiosemicarbazone compounds (Figure 2-1)[24-28]. These other reported Au(III)

thiosemicarbazone compounds all contain an aromatic group. This probably aids in the overall stability of the Au(III) compound. Expanding the carbon backbone in the bis-thiosemicarbazide ligand from 2 to 3 or 4 may provide added stability. However, further investigation has shown that expanding the carbon backbone does not aid in stabilizing Au(III) from reduction[29].

Gold in both the acid form and the tetrabutylammonium (TBA) form yielded the desired product. For radiochemical studies, the TBA form proved better suited for characterization. On the macroscopic, non-radioactive level, the use of TBA hindered [Au(ATSM)]$AuCl_4 \bullet$ 2MeOH crystal growth as well as NMR characterization. When growing crystals using a vapor diffusion method, the crystals that grew after a few days were colorless. These crystals were analyzed and shown to be the TBA compound with a hydroxyl group. Samples were analyzed by ^{1}H-NMR and showed traces of TBA. These peaks overlapped the peaks of the coordinated Au(III) complexes. Crystal growth starting with $NaAuCl_4$ with ATSM ligand was difficult too. Numerous attempts to grow X-ray quality crystals of [Au(ATSM)]$AuCl_4 \bullet$ 2MeOH resulted in a colorless crystal which turned out to be the ATSM ligand. Table 2-1 below shows the crystal data for this compound.

Table 2-2 compares [Au(ATSM)]$AuCl_4 \bullet$ 2MeOH with the more studied Cu(ATSM). The bond lengths and angles are quite similar. The major difference between the two compounds is the C-S bond length is slightly longer when Au(III) is complexed rather than Cu(II). Also, since Au(III) is a larger ion than Cu(II) the metal to sulfur and to nitrogen bond lengths are also longer.

Both of these Au(III) bisthiosemicarbazone complexes are very insoluble except in alcohols and DMSO. This problem was also seen with the Zn(ATSM)[30]. Even in a DMSO solution, both Au(ATSM/PTSM) become unstable when water is added resulting in a heavy white precipitation. From the ^{1}H-NMR spectra of [Au(ATSM)]$AuCl_4 \bullet$ 2MeOH, the presence of ammonium was indicated by three singlets from 7 to 7.3 ppm. Attempts to obtain a ^{13}C-NMR spectrum failed due to the instability of the complex in DMSO-d_6, which can be observed from the gradual color change from purple to yellow indicating reduction of Au(III) to Au(0). In a radiochemical study, ultra pure DMSO was used in an attempt to stabilize Au(ATSM/PTSM) compounds. However, over the course of a few months colorless crystals were observed sitting in a faint yellow solution. X-ray analyses were performed only to reveal the uncomplexed ligand.

Both Au(ATSM/PTSM) compounds can be easily purified by filtration through glass wool. The compounds are less likely to degrade if the solvent used is methanol, not ethanol. This is especially true for the Au(PTSM) compound. Based on other studies on Cu(PTSM)[31], we found that the addition of ethyl acetate resulted in a higher product yield.

The bond lengths of Au-S and Au-N of other reported Au(III) thiosemicarbazones are 2.194-2.266 Å and 1.904-2.130 Å, respectively [24-28]. The Au-S bond of the complex is slightly longer at 2.275-2.281 Å. Whereas, the Au-N bond length is in agreement with the other reported Au(III) thiosemicarbazones. In addition, the bond angles about the Au(III) center is quite distorted, which may also contribute to its instability.

These results have provided insight on the chemistry of Au(III) bis-thiosemicarbazone macrocycles. Bottenus et al[29] conducted studies on increasing the

ligand backbone from an ethylene to a propylene and to a butylene backbone in an attempt to aid in the ability to complex and stabilize Au(III) from reduction. The ethylene backbone with more functional groups from the side chains were found to be the most stable to complex the Au(III) metal center from reduction. Another possibility to explore would be to incorporate aromatic groups or to fuse multiple thiosemicarbazones together creating one large ligand as previously reported[25-28, 32].

Of the two Au(III) complexes, Au-ATSM appears more stable. When purified solutions of Au-ATSM and Au-PTSM are allowed to sit, the color change from purple to yellow over time occurs faster with Au-PTSM. The only structural difference between the two ligands is an extra methyl group off the two carbon backbone for ATSM. The use of various solvents from ethanol, methanol, DMSO, ethyl acetate, to acetone reveals the same instability. Surprisingly, in one microscale radioactive synthesis of ^{198}Au-ATSM in pure DMSO resulted in a crystal structure of just the ATSM ligand in a yellow solution. At first we speculated that the instability might be due to impurities in the ligands or DMSO. Further purification of both PTSM and ATSM ligands by using hot ethanol revealed the same outcome. Even using a freshly prepared batch had the same result.

Both Au(III) complexes are highly colored even at low concentrations (~0.018 mM Au). At these low concentrations, the Au(III) complexes appear pink in solution. Their stability is generally poorer than at macroscopic levels. Over a 24 hour period, the pink color becomes fainter and eventually turns yellow. Radio-TLC confirmed the degradation. In addition, both Au(III) complexes are more stable in methanol versus

ethanol. Several reactions were run using just pure ethanol or pure methanol. Ultimately, ethanol was favored over methanol because it was compatible *in vivo*. As the crystal structure of [AuATSM]$AuCl_4 \bullet$ 2MeOH shows, ethanol could be too big of a molecule to provide suitable stability as opposed to methanol. In growing these crystals, any solution containing ethanol degrades over time at a faster rate than in methanol. One explanation could be that methanol is smaller than ethanol which allows for this crystal to form.

Au-ATSM and Au-PTSM stability in PBS was very poor. Just one drop in PBS would cause the colorless PBS solution to turn cloudy. It was determined that the cloudiness was due to hydrolysis of the ligand. $HAuCl_4$, $NaAuCl_4 \bullet 2H_2O$, TBA-$AuCl_4$, and DMSO did not cause a cloudy precipitate to form in PBS.

Bottenus et al.[29] synthesized another Au(III) bis-thiosemicarbazone, [^{198}Au][Au(3,4-HxTSE)$^+$], and determined its stability in PBS was > 80% after 24 h. This Au(III) complex has 4 ethyl groups off the carbon backbone and terminal amines. The 3,4-HxTSE ligand, like the ATSM ligand, is symmetrical. Symmetry may have an important role in stabilizing the Au(III) center.

Bottenus et al.[29] performed biodistribution studies in normal CF-1 mice using the control [^{198}Au]$AuCl_4^-$ and [^{198}Au][Au(3,4-HxTSE)$^+$] to determine *in vivo* stability by intravenous injection through the tail. High lung accumulation was reported in both compounds, although it was much higher for [^{198}Au][Au(3,4-HxTSE)$^+$] (Tables 2-2 and 2-3). This could be from the decomposition of [^{198}Au]$AuCl_4^-$ and [^{198}Au][Au(3,4-HxTSE)$^+$] in which the ^{198}Au(III) is bound to serum proteins which contains the sulfur

containing amino acid cysteine. The resulting ^{198}Au-protein species maybe over 10 μm, as this would explain why there was a large accumulation in the lungs.

Appendix Chapter 2

Figure 2-1. Other Tri- and Bi-dentate Gold Thiosemicarbazones

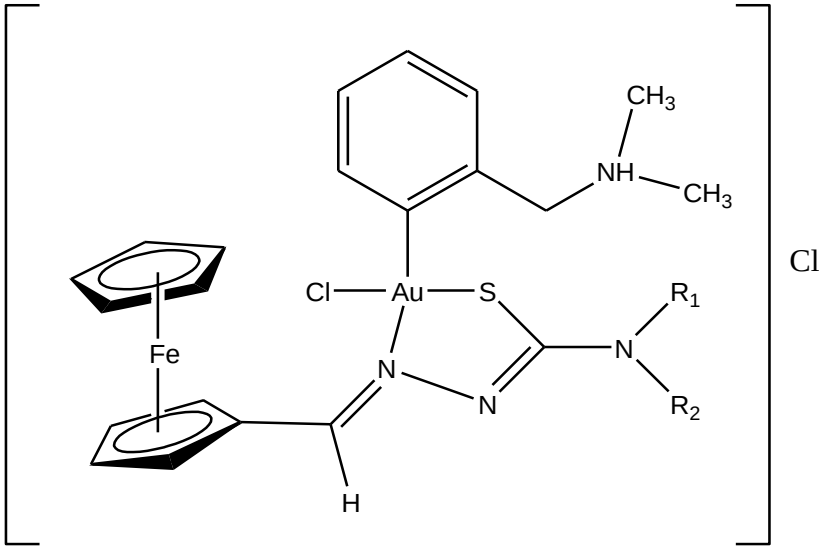

R_1 = H or Me
R_2 = H, Me, Ph, or Et

Casas et al. *J. Inorg. Biochem.* **2004**, *98*, 1009.

Figure 2-1 (continued).

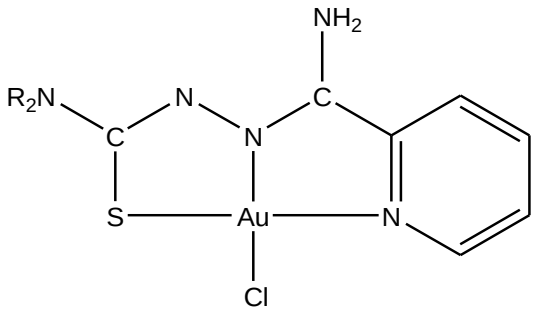

R_1	R_2
H	H
H	Me
Me	Me
$=R_2 = (CH_2)_6$	$=R_1 = (CH_2)_6$

Santos et al. *Dalton Trans.* **2004**, 677

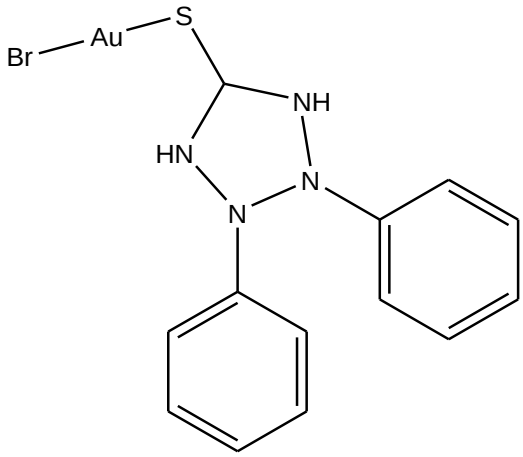

Santos et al, *Dalton Trans.* **2004**, 677

Table 2-1. Crystallographic Data Collection Parameters for [Au(ATSM)]$AuCl_4$·2MeOH

	[Au(ATSM)]$AuCl_4$·2MeOH
Formula	$C_{10}H_{22}Au_2Cl_4N_6O_2S_2$
Formula weight	858.19
Crystal system	monoclinic
space group	P 21/n
a (Å)	14.7293(13)
b (Å)	7.7432(7)
c (Å)	20.4363(18)
α(°)	90
β (°)	100.140(2)
γ(°)	90
V ($Å^3$)	2294.4(4)
Z	4
ρ_{calc}, g/cm^3	2.484
T, K	173(2)
μ, mm^{-1}	13.439
λ source (Å)	0.71073
R(*F*)	0.0393
$R_W(F)^2$	0.0799
GoF	1.048

$R = (\Sigma||F_O| - |F_C||/\Sigma|F_O|)$. $R_W = [\Sigma\varpi(|F_O^2| - |F_C^2|)^2/\Sigma\varpi(|F_O^2|^2]^{1/2}$.

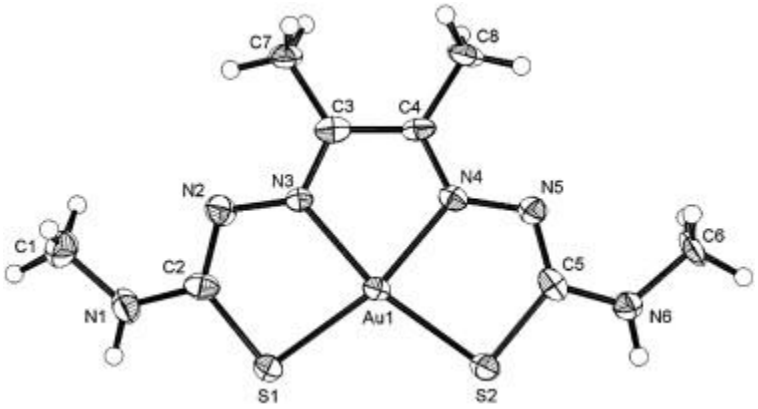

Figure 2-2. ORTEP representation of the [Au(ATSM)]+ cátion with 50% ellipsoids. (Cambridge Crystallographic Data Centre # CCDC 743594).

Table 2-2. Selected Bond Distances (Å) and Bond Angles (deg) for [Au(ATSM)]$AuCl_4$·2MeOH

	[Au(ATSM)]$AuCl_4$·2MeOH
Au-S(1)	2.281(2)
Au-S(2)	2.275(2)
Au-N(3)	2.005(7)
Au-N(4)	2.016(7)
S(1)-Au-S(2)	108.29(8)
N(3)-Au-N(4)	81.3(3)
N(3)-Au-S(1)	84.9(2)
N(4)-Au-S(2)	85.5(2)
N(3)-Au-S(2)	166.8(2)
N(4)-Au-S(1)	166.2(2)

Table 2-3. Biodistribution of [^{198}Au]$AuCl_4^-$ (n=3) in %ID/g[29]

Tissue/organ	15 min	1 h
Blood	22.06±1.56	19.66±7.42
Heart	8.06±1.58	6.91±1.67
Lung	10.28±1.76	11.99±1.58
Liver	6.08±0.62	5.99±2.61
Kidneys	10.13±1.05	17.24±7.77
Spleen	4.98±1.45	5.17±3.60
Stomach	1.28±0.27	2.08±0.47
Small intestine	2.17±0.29	3.08±1.70
Large intestine	1.23±0.27	2.02±0.98
Muscle	2.29±0.24	2.88±0.87
Bone	3.50±0.76	3.57±1.25
Brain	1.08±0.33	0.77±0.27
Pancreas	4.21±0.46	5.08±1.88

Table 2-4. Biodistribution of [^{198}Au][Au(3,4-HxTSE)$^{+}$] in %ID/g[29]

Tissue/organ	15 min	1 h	4 h
Blood	27.14±2.89	27.79±1.21	26.26±4.95
Heart	9.99±2.13	8.44±1.15	8.50±1.60
Lung	73.57±11.47	65.56±11.57	39.44±5.24
Liver	5.13±0.85	4.59±0.78	4.21±0.79
Kidneys	9.41±1.82	9.30±1.75	8.35±1.63
Spleen	9.17±2.00	9.09±2.87	7.64±1.16
Stomach	1.23±0.38	1.57±0.80	1.26±0.35
Small intestine	1.65±0.43	1.98±0.50	1.71±0.28
Large intestine	0.61±0.19	0.58±0.05	1.73±0.56
Muscle	1.35±0.22	0.92±0.16	1.55±0.37
Bone	1.84±0.40	1.36±0.81	1.73±0.58
Brain	0.89±0.20	0.85±0.73	0.69±0.16
Pancreas	2.80±0.67	2.62±0.48	2.54±0.64

Chapter 3: Gold Nanoparticle Syntheses with Gum Arabic, Starch, and Epigallocatechin Gallate (EGCG) as Stabilizers and Their Biodistribution in PC-3 (Human Prostate Carcenoma) Bearing Mice

3.1 Introduction:

Cancer is a worldwide epidemic that affects people from all backgrounds. According to the American Cancer Society, cancer is caused by internal factors (inherited mutations, hormones, immune conditions, and metabolism mutations) and external factors (tobacco use, certain chemicals, high radiation exposure, and certain infections)[33]. If detected early, the effectiveness of cancer treatments is dramatically increased. Treatment options include surgery, radiation, chemotherapy, hormones, and immunotherapy; each method has its benefits and disadvantages depending on the circumstances. Some problems with conventional therapies include side effects, biocompatibility, and toxicity. Incorporating nanotechnology into drug delivery systems can minimize or even eliminate toxicity to non-targeted cells. Nanoparticles with sizes ranging from 1 nm to 100 nm can enter small capillaries and can go undetected by the immune system. Some can pass through the blood brain barrier allowing for brain imaging or even treatment of brain cancer [34]. Since 1990, scientific publications pertaining to nanoparticles have grown exponentially, with a majority of the publications relating to gold nanoparticles (AuNPs) [35].

The attention that AuNPs receive can be attributed to their unique optical properties, the ability to functionalize their surface, and relatively easy production. AuNPs are much different than their bulk counterparts. Bulk gold is a bright, lustrous yellow and very inert, whereas, AuNPs can be red, purple, or blue in aqueous solution

depending on their size and very reactive if not encapsulated by a stabilizer. Bulk gold metal has a melting point of 1064^{o}C, whereas AuNPs of approximately 2 nm in size melt at ~200^{o}C [36, 37]. Smaller size AuNPs (1 to 40 nm) will appear red due to interaction of light with its Surface Plasmon Resonance (SPR). Medium size AuNPs (40 to 80 nm) will appear purple. Larger size AuNPs (+80 nm) will appear blue. The structure within the core of AuNPs has been shown to be face centered cubic packing, similar to that of bulk gold [38]. However, on the surface the packing is more disordered, which explains why stabilizers are required to prevent agglomeration [38].

Stabilizers and reducing agents play an important part in designing AuNPs for a specific size, shape, and monodisperity [35]. AuNPs have a broad spectrum of potential applications. Researchers are currently looking at their uses in chemical and biological sensing [39-41], cancer diagnosis and treatment [34, 42, 43], catalysts [44, 45], and various electronic applications [46-48]. All these uses require the appropriate stabilizer. For *in vivo* applications, the stabilizer should be non-toxic and not degrade in the bloodstream. The addition of dendrimers and polyethylene glycol (PEG) to the surface of AuNPs has been shown to aid in functionalization and reduce absorption or uptake within normal tissues.

The size of AuNPs can provide a better understanding of biological systems since most proteins are generally on the order of tens of nm in size. For instance, incorporating Au in nanostructures can allow for drug delivery agents, labeling agents, and sensors. Size plays an important role in aqueous media. As their size approaches 100 nm, the color will appear more bluish. AuNPs with a diameter around 10 nm appear ruby red in aqueous solution. The desired size will depend on what the application is.

In this thesis, the use of 3 stabilizers is studied (starch, gum Arabic, and epigallocatechin gallate (EGCG)) for biodistribution studies in human prostate cancer (PC-3) bearing SCID mice. Starch is a natural carbohydrate found readily in plants. Gum Arabic is a glycoprotein derived from Acadia trees and used as an additive in many foods. EGCG is a natural anti-oxidant found in green tea. All 3 stabilizers are water soluble and non-toxic.

3.2 Materials:

Starch was purchased from Acros and used without further purification. Gum Arabic was obtained from Sigma-Aldrich. Epigallocatechin gallate (EGCG: > 95% purity) was obtained from Alexis (San Diego, CA). Au foil (> 99.9%), Pt foil (> 99.95%) and $NaAuCl_4 \bullet 2H_2O$ (> 99%) were purchased from Alfa Aesar. All water used was 18 MΩ and purified by a Millipore filtration system in-house. All acids and bases were Optima grade and purchased from Fisher. Sephadex G-100 Superfine was purchased from GE Healthcare. Tris-hydroxylmethyl phosphine alanine (THPAL) was synthesized according to the literature [49]. All chemicals were used as received with no further purification.

3.3 Experiment:

Starch-AuNP

Six mL of water was heated in a 20-mL glass LSC (liquid scintillation counting) vial to ~90^{o}C. Starch (3.75 mg) was added. The mixture was stirred for 3 min while maintaining a temperature near 90^{o}C. The starch had to be fully dissolved and the solution had to be transparent with no signs of discoloration. If the solution was discolored, a new batch of starch solution had to be prepared.

$HAuCl_4$ was prepared by dissolving 2 mg of Au foil in 600 to 800 μL of aqua regia (3 HCl: 1 HNO_3) with heating. Dissolving the Au foil turns the aqua regia yellow. The aqua regia was then heated to near dryness leaving approximately 10 to 30 μL remaining. 600 to 800 μL of 0.05 M HCl was added and heated to near dryness again to azeotrope off any HNO_3 remaining from the aqua regia. The Au solution was allowed to cool to room temperature before adding 1.0 mL of 0.05 M HCl to make a 0.1 M $HAuCl_4$ (2% w/v $HAuCl_4$) solution.

THPAL (mol. wt. 338) was dissolved in water to prepare a 33.7 mg/mL solution. Once the starch solution had been prepared, $HAuCl_4$ (0.1 M, 100 μL) was immediately added with stirring along with 20 μL of THPAL solution. The molar ratio of $HAuCl_4$ to THPAL was 1:5. A color change was observed going from yellow to purple. The solution was stirred for 30 min before filtration by size exclusion chromatography (SEC) using Sephadex G-100 Superfine resin. 9-cm poly prep BioRad columns were washed with water prior to loading. 300 mg of resin was slurred in for each column. Two SEC

columns were used for each starch-AuNP reaction. Each column had a void volume of 2 mL which allows for filtering of 2 mL of starch-AuNP per column.

Gum-AuNP

Six mL of water was heated in an LSC vial to 90^{o}C. Gum Arabic (3 mg) was added to the hot water. Then, 100 μL of $HAuCl_4$ (0.1 M) was added, immediately followed by 20 μL of THPAL solution. The molar ratio of $HAuCl_4$ to THPAL was 1:5. A color change from yellow to purple was observed instantly. The solution was immediately removed from the heat source and allowed to cool to room temperature while stirring for 30 min.

EGCG-AuNP

EGCG (2.0 mg) was added to 6 mL of water and allowed to stir at room temperature for at least 3 hours to ensure complete dissolution. A solution of 0.1 M $AuCl_4^-$ in water was made by dissolving 78 mg of $NaAuCl_4 \bullet 2H_2O$ in 2 mL of water. 100 μL of this Au solution was then added to a stirring EGCG solution. The EGCG provided a dual role as a reducing agent and as a stabilizer.

Radioactive ^{198}Au/^{199}Au Nanoparticle Syntheses

Natural Au foil (0.05 mg to 0.12 mg) was irradiated 12 to 72 h with a thermal neutron flux of 8 x 10^{13} n/cm^2/s and an epithermal neutron flux of 4 x 10^{12} n/cm^2/s. For ^{198}Au, irradiated Au foil from MURR was dissolved similarly to the procedure mentioned

above in a glovebox. The exception was that the mass of the irradiated Au foil was small, and the solution was kept as concentrated as possible.

Production of $^{198}Au/^{199}Au$:

$$^{197}Au + {}^{1}n \rightarrow {}^{198}Au \rightarrow {}^{198}Hg + \beta^{-}$$

$$^{198}Pt + {}^{1}n \rightarrow {}^{199}Pt \rightarrow {}^{199}Au + \beta^{-}$$

For ^{199}Au, natural Pt foil was irradiated similarly to the procedure above. Natural Pt foil (1.2 to 5 mg) was irradiated for 2 to 5 days. HCl (3 M) was used instead of 0.05 M HCl. This procedure is more thoroughly described in the literature [50]. Two chemical species were formed, $H^{199}AuCl_4$ and $H_2{}^{191, 193, 193m, 195, 195m, 199, \text{ and } 199m}PtCl_6$. $H^{199}AuCl_4$ was separated using solvent extraction with an equal volume of ethyl acetate. The extractions were performed at least 30 min after irradiation so that the maximum activity of Au-199 from Pt-199 could be obtained. HPGe analyses were performed during each extraction to verify that no Pt breakthrough was observed. Usually 2 to 3 extractions were required to remove > 90% of the Au-199.

The ethyl acetate extractions with Au-199 were combined and counted on the HPGe detector. If any noticeable Pt breakthrough was observed, the ethyl acetate had to be completely evaporated. 3 M HCl was added, and extractions were performed again using ethyl acetate. If no Pt breakthrough was observed, the ethyl acetate extractions were completely evaporated. A small amount of 0.05 M HCl was added (< 200 μL).

Radiochromatography was performed on the purified $H^{199}AuCl_4$ in 0.05 M HCl. Cellulose TLC paper was spotted and developed in methanol with a drop of concentrated HCl and provided consistent results with the literature [19]. $H^{199}AuCl_4$ is mobile (R_f ~ 0.8 to 0.9) and any colloidal ^{199}Au will remain at the origin. If no colloidal ^{199}Au was present, this solution was added to a carrier $HAuCl_4$ or $NaAuCl_4$ solution (0.1 M Au). This spiked solution was used in place of non-radioactive $HAuCl_4$ or $NaAuCl_4$ in the AuNP procedures described above. More details concerning actual activities, volumes, precautions, etc. will be described in the next chapter.

3.4 Characterizations:

All non-radioactive AuNPs were characterized by optical spectroscopy and electron microscopy. Radioactive AuNPs were characterized by optical spectroscopy and radiochromatography. Analyses on starch-, gum-, and EGCG-AuNP using optical spectroscopy revealed maximum absorptions at 540 to 545 nm, 540 to 560 nm, and 525 to 530 nm, respectively. The filtered starch-AuNPs would have a maximum absorption of 535 to 540 nm, generally 5 nm less than the crude starch-AuNP.

For particle size analysis, AuNP samples were deposited on a copper carbide grid. Any excess was removed by using a tissue paper. The grid was then analyzed using TEM (transmission electron microscopy) or STEM (scanning/transmission electron microscopy) and indicated that the starch-AuNP ranged from 40 to 60 nm in size (Figure 3-1). Gum-AuNP ranged from 50 to 80 nm in size (Figure 3-2). EGCG-AuNP ranged

from 30 to 40 nm in size (Figure 3-3). The filtered starch-AuNP ranged from 25 to 35 nm in size (Figure 3-1).

In Vivo Gum-^{198}AuNP and EGCG-^{198}AuNP Biodistribution Studies

Twenty-five SCID (severely compromised immune deficient) mice bearing a flank model of human prostate cancer derived from a subcutaneous implant of 10 million PC-3 cells were used for all pharmacokinetic studies. Injections were done IV (intravenous), IP (intraperitoneal), and IT (intratumoral). For the IV and IP studies, 40 to 50 μL of gum-^{198}AuNP (3.5 to 7.0 μCi) were injected into each tumor, whereas with the IT study, 30 to 40 μL (3.5 to 7.0 μCi) were injected. Five mice were humanely sacrificed by cervical dislocation at each of the following time points: 30 min, 1 h, 2 h, 4 h, and 24 h. Organs, blood, feces, carcass, and urine were removed, weighed, and counted on a gamma counter. Au-198 activity was decay corrected. Au-198 accumulation per organ is represented as the percentage of injected dose per gram of the organ. Error analysis used was standard error of the mean.

For therapeutic studies, SCID mice bearing a flank model of human prostate cancer derived from a subcutaneous implant of 5×10^6 PC-3 cells were used. These unilateral solid tumors were allowed to grow for 3 weeks, and animals were randomized at day 0 into control and treatment groups (n = 7) with no significant differences in tumor volume. On day 8, 30 μL of gum-^{198}AuNPs (408 μCi) was injected directly into the tumor to deliver an estimated dose of 70 Gy. Control SCID mice received 30 μL DPBS. Tumors were then measured twice each week using digital calipers.

3.5 Results and Discussions:

The interaction between AuNP and light provides a reliable means of size determination. How the light is scattered and absorbed depends on the density and size of the AuNPs [51, 52]. The UV-Vis absorption spectra of interest for AuNPs range from 520 to 600 nm. Smaller size AuNPs absorb light at lower wavelengths near 520 to 530 nm. The AuNP solution appears red. For larger size AuNPs the opposite is true, with maximum absorption near 560 to 600 nm. These particles appear blue in solution. Based on our results, if a blue solution of AuNP is observed, it indicates that the sizes are over 100 nm with a very high size variation (i.e., standard deviation). Over a few minutes to a few hours, precipitation can be observed.

One approach to reduce aggregation of AuNPs in solution is to use a lower concentration of Au. Using a high Au concentration increases the number of interactions per Au atom, which can induce colloidal Au even before a reducing agent is introduced. From our experiments of starting with a 2% $AuCl_4^-$ solution, there did not seem to be any difference. However, with the starch- or gum-AuNP, if too much reducing agent was added, the AuNPs would turn blue and precipitate from solution.

Further studies were conducted on gum-AuNP, varying the amount of THPAL reducing agent from 20 μL per 6 mL reaction to 5 μL, 10 μL, and 50 μL, which corresponds to molar ratios of 1:1.25, 1:2.5, and 1:12.5 $HAuCl_4$:THPAL, respectively. The amount of reducing agent has a critical role in the overall size of the gum-AuNPs formed and the reaction time. Using only 5 μL or 10 μL of THPAL provided a greater

size disparity, generated a lower concentration of gum-AuNPs, and more aggregation was observed in a short period of time (several min). This effect was reported in the literature for another AuNP method where trisodium citrate was used in varying concentrations to reduce tetrachloroauric acid under the Turkevich method[53]. At 50 μL of THPAL, the gum-AuNP solutions were less likely to aggregate and had the highest concentration of nanoparticles as confirmed by UV-Vis spectroscopy and TEM. This could be due to reducing $HAuCl_4$ vs. $NaAuCl_4$. The acidity could have some effect on the reducing potential of THPAL.

For the EGCG-AuNP, the pH of the $AuCl_4^-$ was extremely important. The original procedure called for using a 2% Au solution of $NaAuCl_4 \bullet 2H_2O$. The pH of this gold(III) solution was between 2 to 3. For radioactive EGCG-^{198}AuNP, a 2% Au solution of Au metal dissolved in aqua regia and reconstituted in 0.05 M HCl had a pH of 0 to 1. If a simple substitution of using 2% of Au solution from Au metal for $NaAuCl_4 \bullet 2H_2O$ were used, the EGCG-AuNP solution would turn a cloudy purple. The EGCG-AuNP solution would precipitate from solution in a few hours. Some adjustments that were made involved adjusting the pH of the EGCG solution to be more basic. In a basic environment ($pH \leq 10$), the EGCG solution is yellow. Adding the Au solution in 0.05 M HCl would work some of the time, but at times the solution would turn red, then purple, then settle out of solution in a few hours. Some pH adjustments of the 2% Au solution were also made by adding some concentrated NaOH to get the pH near 7. This would again work some of the time. The best method to date is to introduce a small amount (> 10 μL of 2% $H^{198}AuCl_4$) with at least 100 μL of 0.1 M $NaAuCl_4 \bullet 2H_2O$ carrier solution.

Temperature was also critical in synthesizing AuNP. Over heating will cause precipitation to occur. This could be due to the increase in kinetic energy from heating, which would increase collisions between AuNPs. Another reason could be that excess heat causes the stabilizers to decompose, therefore allowing the AuNPs to agglomerate. The EGCG preparation required no heating, but the reaction was very slow. Since the EGCG compound is only slightly soluble in water, a longer stirring time is required (over 1 hour). Once the Au(III) solution was added, the reaction must stir for another hour or two. Otherwise, a radiochromatography analysis would still reveal that free Au(III) was present. The starch- and gum-AuNP preparations were the fastest, usually completed around 30 min to 2 hour from start to finish. The starch-AuNP procedure required a filtration step to remove excess starch in solution, otherwise precipitation will occur.

To determine the percent yield of the reaction, a radiochromatogram on TLC cellulose paper was taken for each experiment. This characterization method was referenced from the literature [19]. Briefly, methanol with one drop of concentrated HCl was used as the developing solution. Free Au ($AuCl_4^-$) migrates in methanol, R_f ~0.7 to 0.9. AuNPs remained at the origin. EGCG-AuNPs yields are > 95%. Gum- and starch-AuNPs have yields that are between 60 to 80%. The yield improves if more THPAL reducing agent is added. The optimum amount is 50 μL of THPAL (33.4 mg/mL) in a 6 mL reaction. Experiments conducted using 100, 80, and 60 μL of THPAL caused agglomeration within a few minutes.

Biodistribution studies were performed on radioactive Au-198: EGCG- and gum-AuNP. Intravenous (IV), intraperitoneal (IP), and intratumoral (IT) studies were

performed. Results showed that high uptake was observed in the lungs (25.20 ± 3.64 %ID/g at 2 h), liver (94.47 ± 13.14 %ID/g at 2 h), and spleen (19.46 ± 4.26 %ID/g at 2 h) for the IV study (Figure 3-4(a)). This uptake pattern was similar to that of larger colloidal particles. The IP study revealed that uptake was very sporadic in the peritoneal cavity (Figure 3-4(b)). The blood clearance was much slower in the IP study than the IV study. From the IP study, blood retention of the gum-^{198}AuNP was at 18.55 ± 7.60 %ID/g at 30 min to 15.95 ± 6.59 %ID/g at 2 h. Blood retention in the IV study was 24.89 + 12.93 %ID/g at 30 min and quickly dropped to 5.54 ± 2.67 %ID/g at 2 h. The IT study showed excellent tumor retention with total tumor accumulation of gum-^{198}AuNP of 154.05 + 18.02 %ID/g at 30 min and 87.73 ± 16.82 %ID/g at 24 h. Any leakage of Au-198 was cleared through the kidneys (Figure 3-4(c)).

Therapeutic applications were further evaluated in 14 SCID mice bearing 5 million PC-3 cells. The mice were randomized into two groups one receiving a placebo (Dulbecco's PBS) and the other receiving ~70 Gy of gum-^{198}AuNP via IT injection. The results concluded that total tumor volumes were drastically decreased after two weeks post-injection of gum-^{198}AuNP (Figure 3-5). The radiation from Au-198 was effective in reducing tumor size. Tumors harvested from the treatment group consisted largely of necrotic tissue, indicating extensive tumor cell kill. These residual tumor tissue samples still contained 19.9 ± 4.2% of the injected dose (ID) of Gum-^{198}AuNPs. Liver contained 0.91 ± 0.26% ID, kidney 0.13 ± 0.01% ID, and small intestines 0.09 ± 0.00% ID. Levels of radioactivity noted for blood, heart, lung, spleen, stomach, and pancreas were barely distinguishable from background, and the remaining carcass contained 18.5 ±

4.6% ID. Insignificant or no radioactivity in liver, intestine, and various non-target organs unequivocally established that the therapeutic payload had remained within the tumor site throughout the 30-day treatment regimen.

Figures 3-6 and 3-7 show the biodistribution uptake of organs from an IT study and a therapeutic study involving EGCG-^{198}AuNPs, respectively. The organ uptake and therapeutic studies were similar to the gum-^{198}AuNP IT studies. IT biodistribution studies revealed that the tumor had a maximum uptake of 440.51 $\pm$ 45.87 %ID/g at 4 h. The lungs accumulated 6.13 $\pm$ 4.54 %ID/g after 24 h. Therapeutic studies with the EGCG-^{198}AuNP showed a decrease in tumor size after administration when compared with the two control groups: Dulbecco's PBS and EGCG solution. The Dulbecco's PBS or EGCG solution indicated no tumor shrinkage. This contradicted the literature reports on EGCG as an anti-tumor agent[54]. The concentration of EGCG (0.37 mg /mL) could be too low to provide any therapeutic effect. This was reported in the literature where an EGCG concentration over 1 μM, or 0.46 mg/mL, were required to elicit anti-cancer activity, which is equivalent to drinking approximately 10 cups of green tea. Combining EGCG with a vitamin A derivative, (all-*trans*-retinoic acid) ATRA, have been shown to reduce tumor growth of B16 melanoma in mice[55]. Vitamin A is found in various foods, such as eggs, meat, milk, cheese, cream, liver, cod, and fish oils. A healthy, balanced diet can be the first line of defense against cancer.

A follow-up study using Au-199 could prove to be beneficial, since the nuclear properties of Au-199 are more ideal for therapeutic applications and its gamma ray emissions are less penetrating. The 411 keV (95%) gamma-ray of Au-198 is very

penetrating and can cause radiation damage to normal tissue. The majority of gamma-rays of Au-199 are within 100 to 200 keV and are more optimal for single photon emission computed tomography (SPECT). Gold-199 also has a lower beta max energy of 0.46 MeV vs. 0.96 MeV from Au-198.

Appendix Chapter 3.

Figure 3-1. STEM of Unfiltered Starch-AuNP (top) and Filtered Starch-AuNP (bottom).

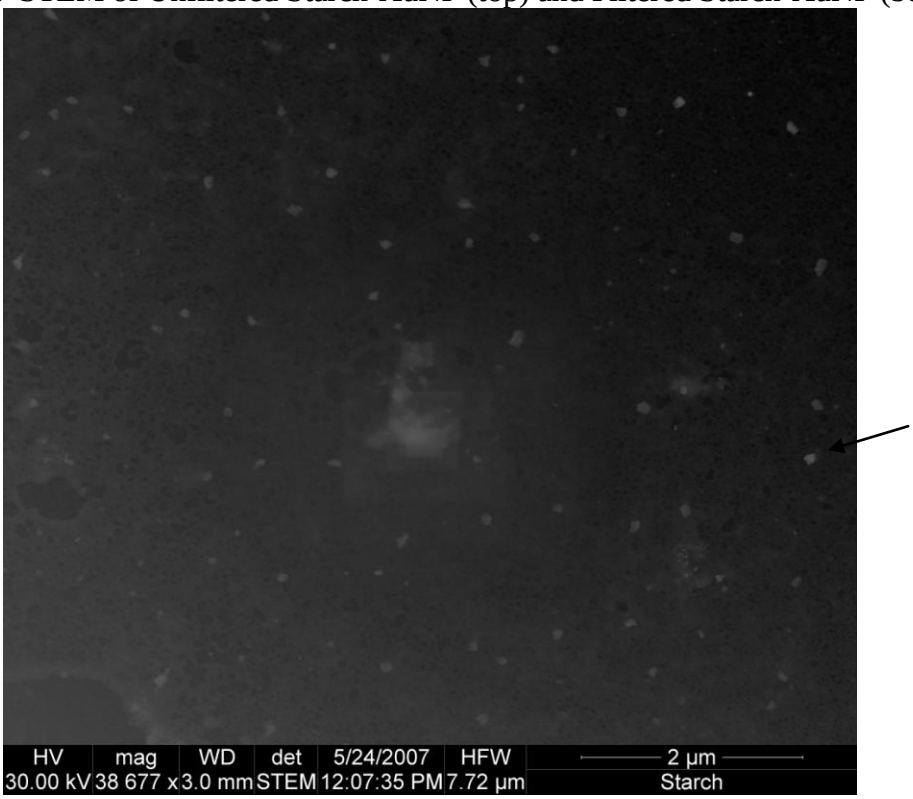

Figure 3-2. TEM (above) and STEM (below) of Gum-AuNP.

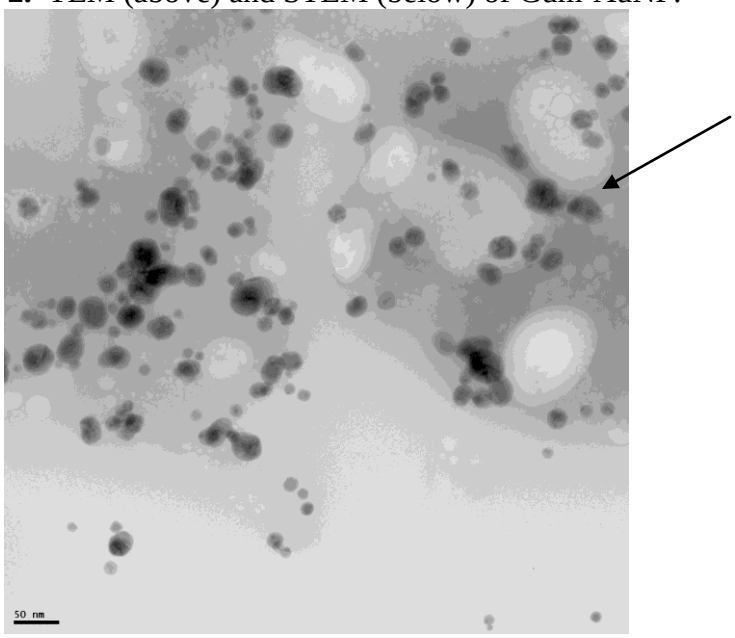

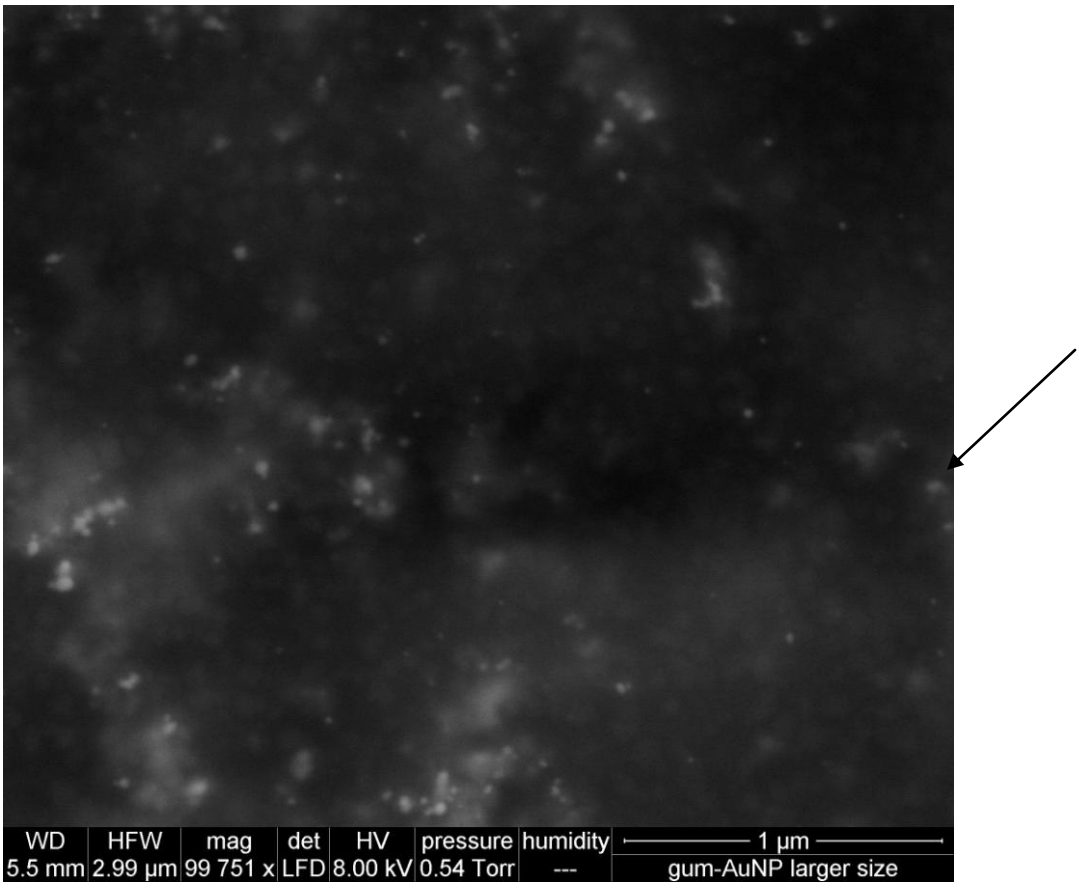

Figure 3-3. TEM of EGCG-AuNP.

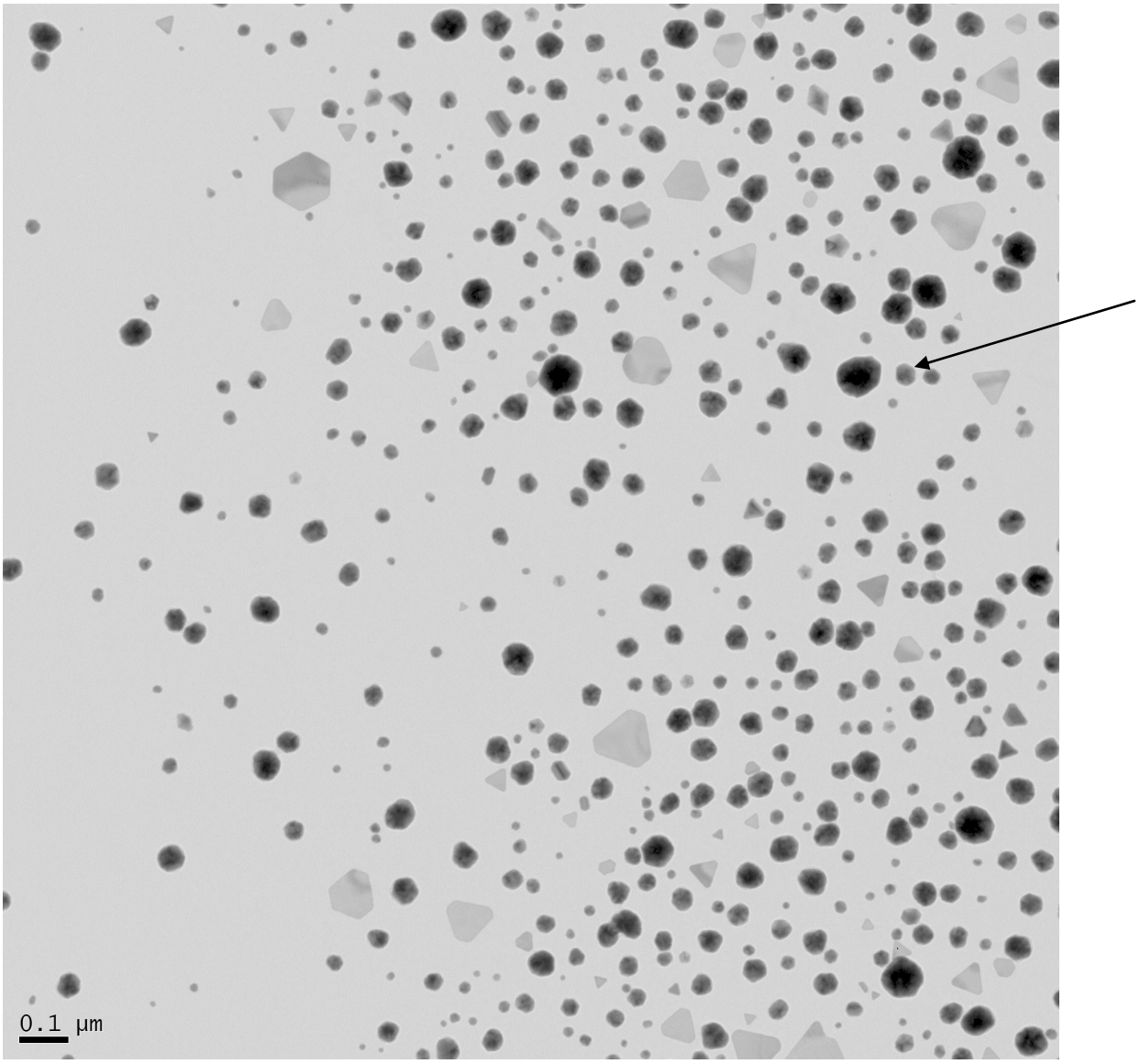

Table 3-1. Size Exclusion Chromatography on Starch-^{199}AuNP.

After 30 min.	$H^{199}AuCl_4$	Starch-^{199}AuNP
Remaining on column	85 μCi	73 μCi
Collected	0	24 μCi

Figure 3-4. Gum-^{198}AuNP Biodistribution Studies in PC-3 Bearing SCID Mice: (a) IV, (b) IP, and (c) IT

(a)

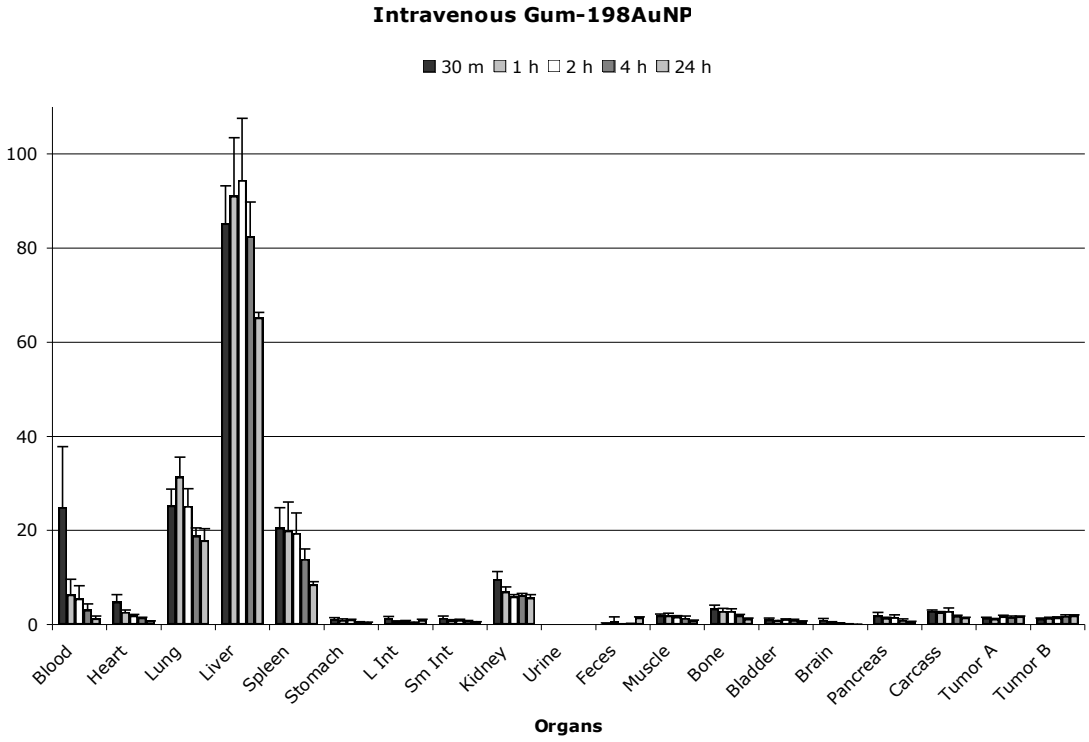

Figure 3-4 (continued).
(b)

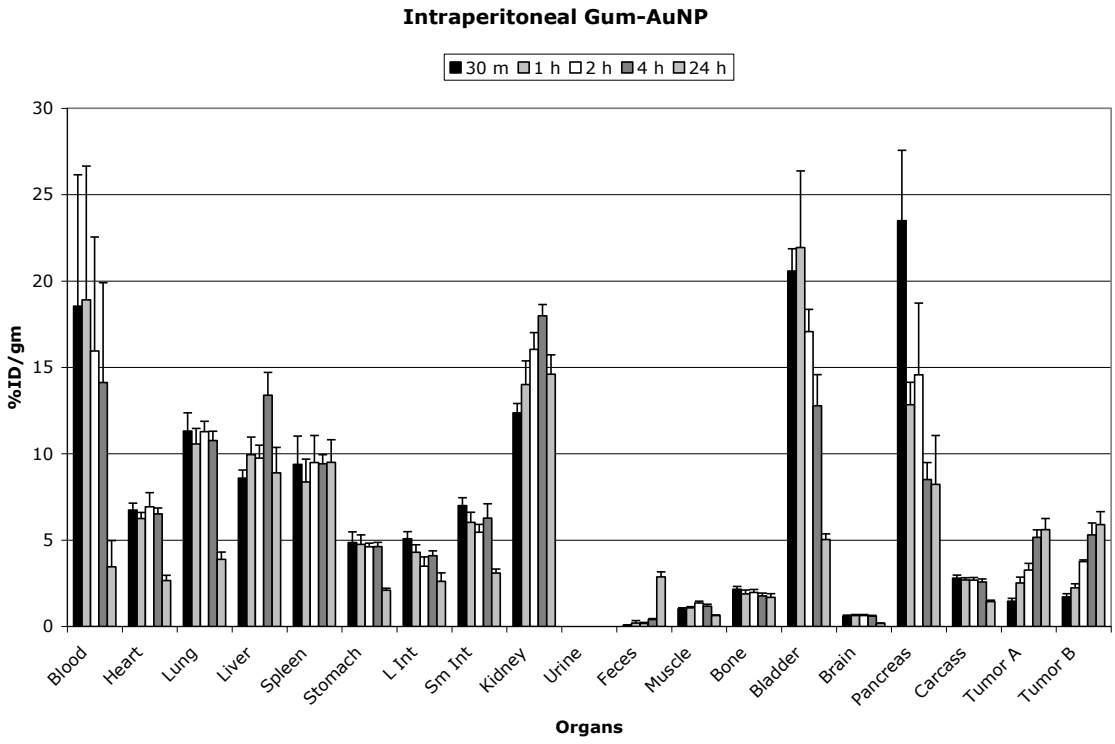

Figure 3-4 (continued).
(c)

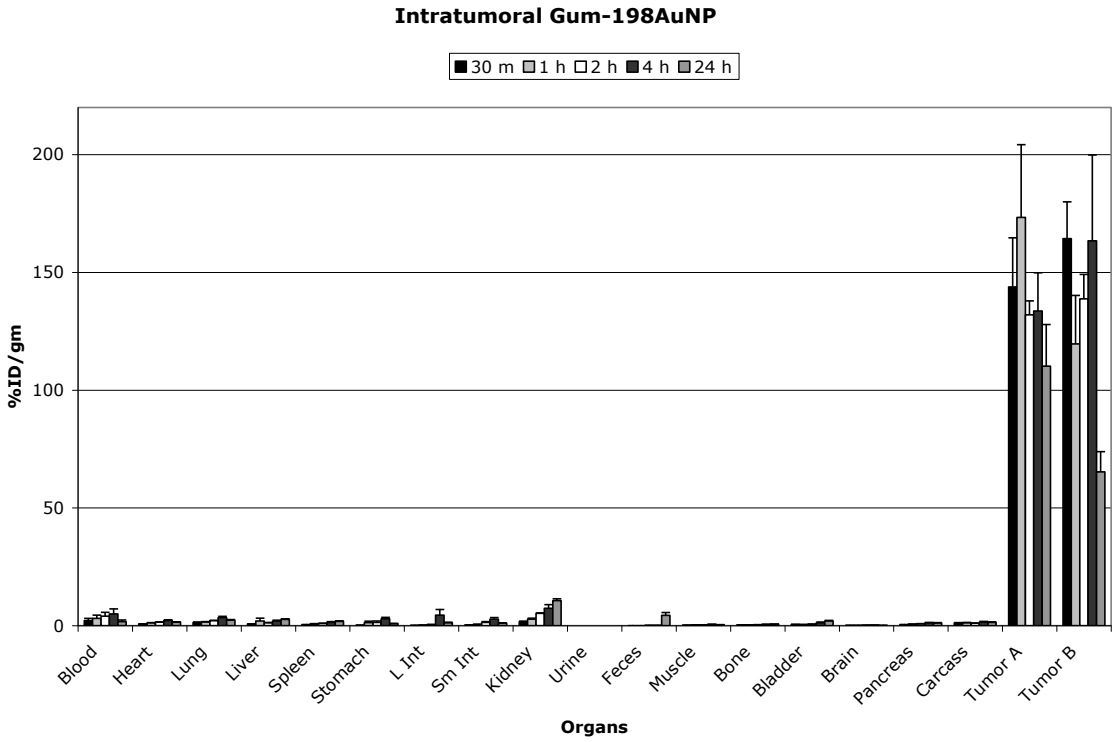

Figure 3-5. Therapeutic Studies with Gum-^{198}AuNP Conducted on PC-3 Bearing SCID Mice.

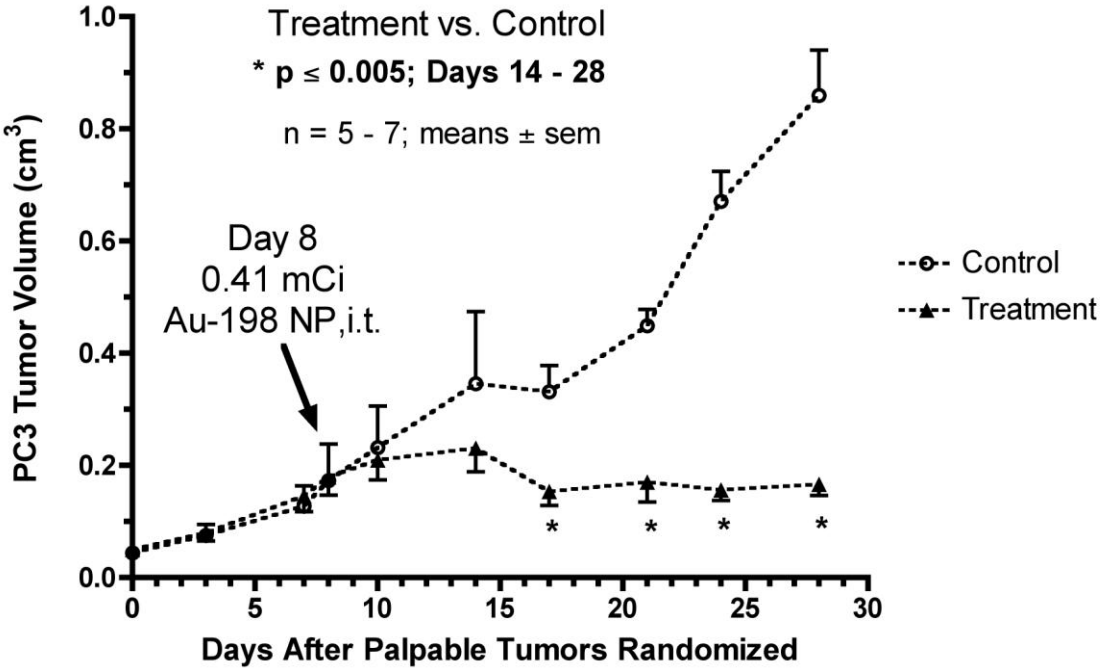

Figure 3-6. EGCG-^{198}AuNP Intratumoral Biodistribution.

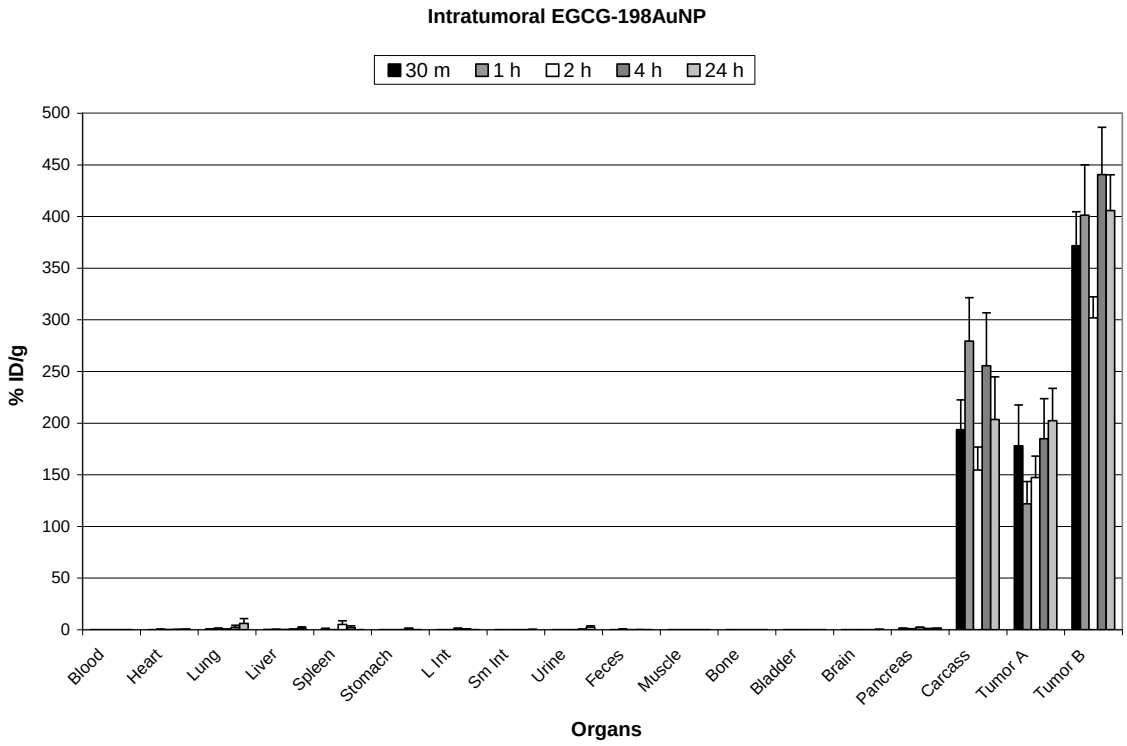

Figure 3-7. EGCG-^{198}AuNP Therapeutic Study.

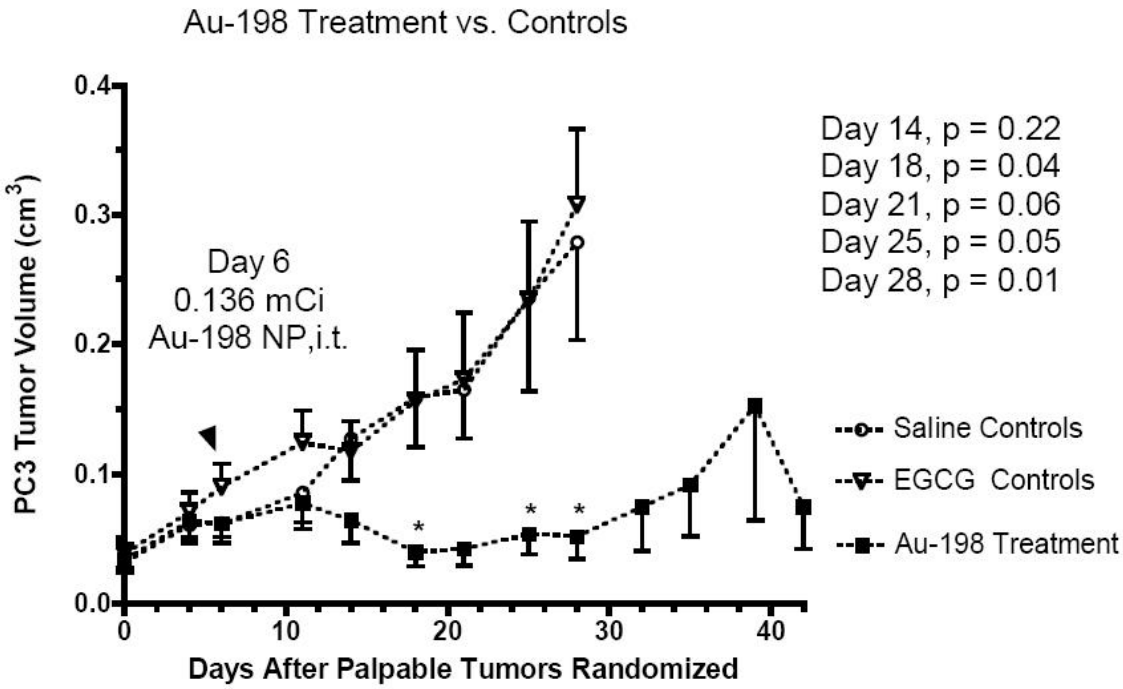

Chapter 4: Targeting PC-3 (Human Prostate Carcenoma) Cells with Starch-^{198}AuNPs (Starch-Stabilize Gold Nanoparticles) Conjugated to Bombesin

4.1. Introduction

In the previous chapters, all research that was performed was on non-targeted gold radiopharmaceuticals. This chapter discusses the targeted approach utilizing starch-^{198}AuNP. Gold is known to have high affinity for sulfur. By using sulfurs bound to a targeting moiety, this can serve as a driving vehicle for the starch-^{198}AuNP *in vivo* towards cancerous cells.

Cancer cells can be targeted by over expressed receptors on their surface. Depending on the type of cancer, these receptors can include TGF-α (transforming growth factor α) [56], TGF-β [57], EGFR (epidermal growth factor receptor) [56, 58-60], somatostatin receptors [61, 62], and GRP (gastrin releasing peptide) receptors [63, 64]. The focus of this chapter is on human prostate cancer (PC-3) cells. These cells have a high concentration of GRP receptors [63]. Literature has also shown that bombesin, an amphibian peptide, has a strong affinity for this receptor [65]. The principle behind this targeting approach is to limit non-specific binding to normal tissue while maximizing uptake in the tumor(s).

Current therapy for localized prostate cancer usually involves brachytherapy, in which radioactive "seeds", a few centimeters in size, are placed in the prostate to kill nearby cancer cells [66]. Approximately 10% of brachytherapy patients do not respond well to this treatment [66]. Of the patients that do respond well, some experience intestinal injury, incontinence, or impotence due to radiation exposure [66]. This treatment is

invasive and requires ultrasound guidance to be accurately placed. A disadvantage to this procedure is that a tumor has to be localized.

In a targeted approach, the cancer does not have to be localized. Bombesin-like receptors are expressed on various cancers including small cell lung, prostate, breast, gastric, colon, and pancreatic[65]. An advantage to using bombesin is rapid clearance from the blood and other non-target tissues due to its relatively small size[67, 68]. The concept is to incorporate numerous bombesin peptides onto the surface of starch-^{198}AuNP. Injection of this radiopharmaceutical through the bloodstream will result in binding to GRP receptors on cancerous cells enabling ^{198}Au to deliver a therapeutic dose that can destroy the cell.

Preliminary studies on non-radioactive starch-AuNP (without bombesin) injected in pigs have shown that these nanoparticles behave like colloidal particles accumulating primarily in the lungs based on NAA (neutron activation analysis) and AAS (atomic absorption spectroscopy)[69].

4.2. Experimental

4.2.1. General

All reagents were used without further purification. Starch was purchased from Acros. Optima grade concentrated HCl, HNO_3, and 10 M NaOH were purchased from Fisher Scientific. Gold metal (> 99.9%) and ultrapure DMSO (dimethyl sulfoxide) were bought from Alfa Aesar. THPAL (tris-hydroxylmethyl phosphine alanine) was

synthesized according to the literature[49]. Thioctic acid linked with bombesin [7-14] (SS-BBN) was purchased from Anaspec.

4.2.2. Physical Measurements

An Ocean Optics UV-Vis USB 2000 spectrometer operated by OOIBase 32 software and a Perkin Elmer Lambda-45 spectrometer operated by UV WinLab 5.1 were used for optical spectroscopy. A Capintec CRC-12 dose calibrator was used to determine radioactivity. All water used was 18 MΩ Milli-Q water distilled in house with a Millipore filtration system.

4.2.3. ^{198}Au Production and Preparation of H^{198}AuCl$_4$

Au foil (0.76 mg; 3.86 x 10^{-4} mol) was irradiated for 3.5 hours producing 20.5 mCi. The irradiated foil was dissolved in 800 μL of aqua regia (3 HCl:HNO_3) in a glass LSC (liquid scintillation counting) vial and heated to near dryness. The dissolution was shielded with lead bricks to reduce the radiation dose. When approximately 200 μL of aqua regia remained, an additional 600 μL of 0.05 M HCl was added and heating was continued to evaporate most of the acidic solution. The Au-198 solution was removed from the heat and allowed to cool to room temperature behind a lead brick. HCl (0.05 M, 200 μL) was added to the Au-198 solution. A drop of this solution was analyzed by radiochromatography using cellulose paper developed in methanol with one drop of concentrated HCl to verify that no colloidal gold-198 was present.

4.2.4. Starch-^{198}AuNP Synthesis and Filtration

A THPAL solution was prepared by dissolving 8.7 mg of THPAL in 258 μL of water. The solution was sonicated for at least 5 minutes. A 3.75 mg/mL solution of starch was prepared by dissolving 84.4 mg of starch with 22.5 mL of water. The solution was heated at 90^{o}C and stirred until the starch was fully dissolved.

Carrier $HAuCl_4$ (0.1 M, 80 μL) was added to the Au-198 (18.4 mCi) solution. The hot starch solution (6 mL) was added, immediately followed by 40 μL of THPAL solution. An immediate color change from yellow to purple was observed, indicating that starch-^{198}AuNP was formed. The solution was allowed to stir for 30 minutes. The sample was analyzed by UV-Vis spectroscopy.

Two size exclusion columns were prepared using Sephadex G-100 superfine resin. Two 9-cm Bio-Rad Poly Prep Columns were rinsed with water. Each column was then loaded with 300 mg of Sephadex G-100 superfine. Water was added to fill the column. The Sephadex resin formed a gelatin inside the column. When all the excess water was eluted from the columns, 2 mL of the starch-^{198}AuNP was added to the column followed by elution with 2 mL of water. The filtered starch-^{198}AuNP was collected and counted against the amount of activity that remained in the columns using a Capintec CRC-12 (Table 4-1).

UV-Vis analyses were performed on pre-filtered starch-^{198}AuNP and filtered starch-^{198}AuNP (Table 4-2).

4.2.5. Starch-^{198}AuNP-SS-BBN Synthesis

SS-BBN (1.4 mg) was dissolved with 2 mL of ethanol in a 10-mL Hollistier-Stier vial. The solution was sonicated for 5 minutes. Once fully dissolved, one mL (752 μCi) of filtered starch-^{198}AuNP from column one was added. The solution was stirred overnight (> 8 h). The reaction was shielded with lead bricks inside a hood minimizing the dose rate at the hood window to under 1 mR/h. A color change was observed from purple to a lavender color. Eventually, a precipitate was observed with little to no purple color in the liquid medium.

The crude starch-^{198}AuNP-SS-BBN was transferred to a 10-mL centrifuge vial. The precipitate was washed with 2 mL of ethanol and added to the centrifuge vial. The activity in the centrifuge vial was 626 μCi. There was 4.2 μCi left in the reaction vial. The starch-^{198}AuNP-SS-BBN was centrifuged for 20 minutes. The ethanol (supernatant) was removed and counted for activity. Then, a fresh 2 mL ethanol aliquot was added to the centrifuge tube and was vortexed and sonicated. The vial was centrifuged again for 20 minutes. This process was repeated to ensure no unconjugated SS-BBN was present (Table 4-3). Washing continued with water using 2 mL per wash three times (Table 4-4). After centrifuging each water wash for 20 minutes, no solid particles were observed. There were only two phases present: (top) colorless ethanol and (bottom) purple color aqueous layer. The top layer was removed leaving the purified starch-^{198}AuNP-SS-BBN.

Ultrapure DMSO (250 μL) was added to the starch-^{198}AuNP-SS-BBN and mixed thoroughly to ensure complete dissolution. Phosphate buffered saline (3.2 mL) was added bringing the total volume of the solution to approximately 3.5 mL. For mice

studies, 3.3 mL of this radiolabeled compound was transferred to a 5-mL conical vial. The vial was crimped and the activity was 126 μCi. The activity per 100 μL dose was 3.5 μCi on the following day, which was when the biodistribution study was performed.

Starch-^{198}AuNP-SS-BBN (300 μL) was diluted with 300 μL of water in a micro volume cuvette. A reference of 7% DMSO in PBS was made. UV-Vis analysis shows a maximum absorption peak at 552 nm.

4.2.6. Starch-^{198}AuNP-SS-BBN Biodistribution Studies in PC-3 Bearing SCID Mice

Twenty-five SCID mice bearing a flank model of human prostate cancer derived from a subcutaneous implant of 10 million PC-3 cells were used for all pharmacokinetic studies. Injections were done IP (intraperitoneal). Five mice were humanely sacrificed by cervical dislocation at the following time points: 30 min, 1 h, 2 h, 4 h, and 24 h. Organs, blood, feces, and carcass were removed, weighed, and counted on a gamma counter. Au-198 activity was decay corrected. Au-198 accumulation per organ is represented as the percentage of injected dose per gram of the organ. Error analysis used was standard error of the mean. This study was conducted by Lisa Watkinson and Terry Carmack at Harry S Truman Veterans Affair Hospital under the supervision of Dr. John R. Lever.

4.3. Results and Discussions

The conjugations of AuNPs with BBN peptide analogs were chosen because the peptide library has demonstrated high affinity toward GRP receptors in vivo

(overexpressed in prostate, breast, and small-cell lung carcinoma). Schally and co-workers have shown that there are 44,000 bombesin receptor sites on human prostate cancer (PC-3) cells[70]. A number of clinical trials in progress are using BBN peptide analogs to target GRP receptors present in prostate cancer for imaging applications[71]. In a human phase-1 clinical study involving radioactive ^{99m}Tc-BBN, the radioactivity was found within 4 min post injection in the prostate tumor region[71].

From the previous chapter involving gum-^{198}AuNP, biodistribution studies were conducted based on 3 administration routes: intravenous (IV), intraperitoneal (IP), and intratumoral (IT). Studies involving the gum-^{198}AuNPs were not conjugated to bombesin to specifically target the GRP receptor of the PC-3 cells. Intratumoral studies showed the best biodistribution result with very little leakage from the tumor. The gum-^{198}AuNPs were shown to clear out through the kidneys with very minor uptake in the liver, spleen, and lungs. In preparation for a targeted starch-^{198}AuNP study, the IP data showed the better biodistribution when compared with the IV. There was more uptake in the pancreas and in the tumors from the IP study than the IV. Therefore, the IP administration route was chosen for this targeted study using starch-^{198}AuNP-SS-BBN. Figure 4-1 shows the biodistribution of starch-^{198}AuNP in comparison with starch-^{198}AuNP-SS-BBN. Both biodistributions are similar in that each radiopharmaceutical mimics colloidal Au uptake by IP injection. There was no significant uptake in the tumors. The pancreas had a maximum uptake at 4 h post injection of 35.70 $\pm$ 20.12 %ID/g. The GRP-receptor density in mice is in the following order: pancreas > tumor > intestine[72]. A recent study has quantified that more than ~300 ($\times 10^3$) bombesin

receptor sites per cell are available in mice pancreas and that prostate tumor PC-3 cells have ~44 ($\times 10^3$) receptor sites per cell[73]. These data imply that GRP-receptor density in pancreas is approximately eightfold higher than that in PC-3 tumors. The sizes of these starch-^{198}AuNP can hinder the binding affinity of bombesin for the GRP receptors on PC-3 cells. The biodistribution studies of starch-^{198}AuNP and starch-^{198}AuNP-SS-BBN are similar to other nanoparticles or colloids. Researchers from Japan studied the biodistributions of citrate-stabilized AuNPs ranging in 15 nm to 200 nm in size after intravenous administration in mice[74]. Their data showed that there was significant uptake in the lungs, liver, and spleen. Semmler-Behnke et al.[75] from Germany, showed the same results comparing 1.4 nm AuNPs and 18-nm AuNPs in rats. Uptake in the liver (> 95% ID/organ) from the 18 nm size AuNP dwarfed those in the spleen and lungs. These AuNPs were surrounded by $Ph_2PC_6H_4SO_3Na$ ligands. To minimize uptake by the liver, lungs, and spleen so rapidly, modification of the surface using PEG (polyethyleneglycol) can be made to increase blood circulation times[76, 77]. PEG modifications on AuNPs minimized non-specific binding to cellular membranes and is a common approach for preparing biocompatible drugs with longer circulating times in the bloodstream[77]. Incorporating PEG to starch-^{198}AuNP-SS-BBN should minimize uptake in non-targeted organs and tissues, which can allow for enough time for the radiolabeled compound to bind to the GRP receptors on the tumors.

Another issue regarding the low tumor uptake of starch-^{198}AuNP-SS-BBN could be the linker size. Thioctic (or lipotic) acid is only a 6-carbon linker between the starch-^{198}AuNP and BBN. This length might be inadequate to provide binding onto the GRP

receptor. Hoffman et al.[78] conducted studies on linker length from the targeting moiety to the radiolabeled compound. A short linker reduces binding affinity because the targeting moiety cannot adequately bind with the receptor. A linker that is too long can also reduce binding affinity because the carbon chain adds hydrophobilicity to the compound. Looking into increasing the space between starch-^{198}AuNP and BBN would be interesting to compare how binding is affected.

Table 4-1(a). Starch-^{198}AuNP Activity Collected vs. ^{198}Au Remaining on the Column.

	Amount collected	Remaining on Column	% Au-198 collected
Column 1	1.50 mCi	3.90 mCi	27.8%
Column 2	1.52 mCi	3.83 mCi	28.4%

Table 4-1(b). UV-Vis Analyses on Starch-^{198}AuNP

Sample	**λ (max)**	**Absorption**
Pre-filtered starch-^{198}AuNP	550	0.9744
Starch-^{198}AuNP (column 1)	546	0.9131
Starch-^{198}AuNP (column 2)	546	0.9155

Table 4-1(c). Ethanol Washes on Starch-^{198}AuNP-SS-BBN

Ethanol washes	**Au-198 breakthrough**
Wash 1	0.5 μCi
Wash 2	5.0 μCi
Wash 3	5.5 μCi

Table 4-1(d). Water Washes on Starch-^{198}AuNP-SS-BBN

Water washes	**Au-198 breakthrough**
Wash 4	356 μCi
Wash 5	69.7 μCi
Wash 6	56 μCi

Figure 4-1. Biodistribution of (a) Starch-^{198}AuNP and (b) Starch-^{198}AuNP-SS-BBN in PC-3 Bearing Mice

(a)

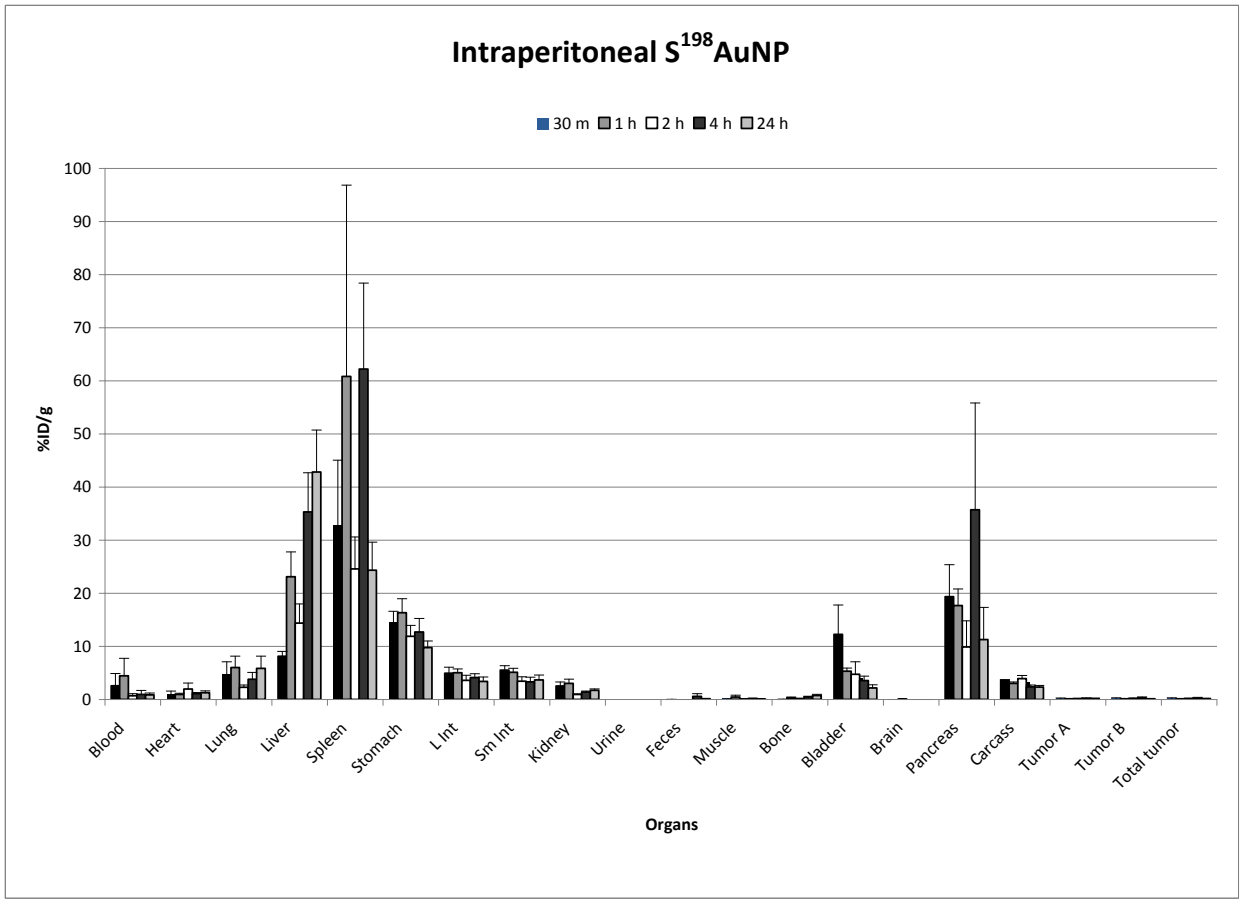

(b)

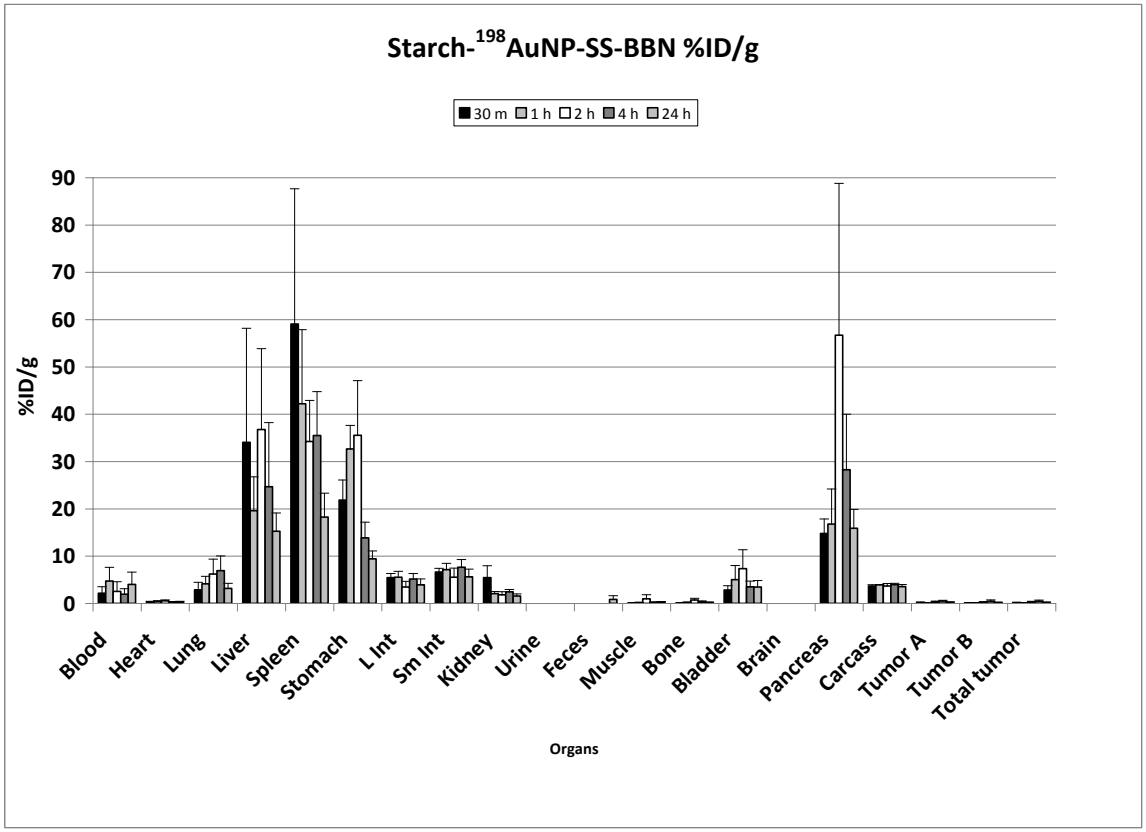
Starch-198AuNP-SS-BBN %ID/g
30 m
1 h
2 h
4 h
24 h
%ID/g
90
80
70
60
50
40
30
20
10
0
Blood
Heart
Lung
Liver
Spleen
Stomach
L Int
Sm Int
Kidney
Urine
Feces
Muscle
Bone
Bladder
Brain
Pancreas
Carcass
Tumor A
Tumor B
Total tumor
Organs

Chapter 5: Future Studies

5.1. Gold (III) bis-thiosemicarbazones

The successful syntheses and characterization of AuATSM[$AuCl_4$] and AuPTSM[$AuCl_4$] provided potential in designing a new chelate that can stabilize a Au(III) compound *in vivo*. A few possibilities to explore to accomplish this problem are outlined below.

A. Incorporating aromatic groups to carbon backbone

Other published literatures of Au(III) thiosemicarbazones contain aromatic groups and are only 2 to 3 coordinate[79-81]. Exploring this possibility can provide insight to stabilizing Au(III) from reduction in aqueous medium.

B. Develop a water soluble thiosemicarbazide ligand

Since both ATSM and PTSM bis-thiosemicarbazide ligands are not soluble in water, determine if a water soluble thiosemicarbazide ligand can coordinate Au(III) and prevent reduction. Fluorecein-5-thiosemicarbazide is commerically available and is soluble in water. Incorporating diacetyl or pyruvic acid to this compound would provide an ATSM or PTSM derivative that should be more water soluble.

Structure for fluorecein-5-thiosemicarbazide

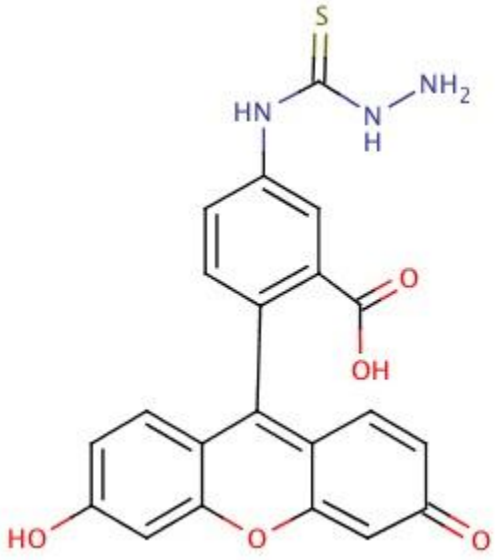

5.2. Gold nanoparticles

Various researchers have shown that gold nanoparticle surfaces can be easily modified to bypass the liver and lungs. Researchers have shown that small charged molecules will clear via the renal system.

A. Evaluate the possibility of using dendrimer stabilized gold nanoparticles to prevent aggregation and to functionalize.

While the starch-^{198}AuNP has a relatively long shelf life in aqueous solution after filtration, the filtration step poses a problem in that most of the activity remains on the column. PAMAM (polyaminoamide) dendrimers have the ability to stablize AuNPs *in vivo* with organ accumulation in the kidneys and bladder[82]. The amides can be functionalized with an appropriate targeting moiety to enable selective binding.

B. Incorporate PEG (polyethylene glycol) into starch-^{198}AuNP-SS-BBN synthesis.

PEG-AuNPs have been shown to reduce accumulation in the liver[77]. This could allow for more circulation throughout the bloodstream which could allow for better accumulation in the tumor.

C. Perform a blocking study on starch-^{198}AuNP-SS-BBN

In order to definitively confirm that uptake in the pancreas was due to selective binding to the GRP receptor, blocking the receptor sites with free bombesin can provide a clear answer.

References:

1. Stapleton, A. E., Ultraviolet radiation and plants: burning questions. *The Plant Cell* **1992,** 4, 1353-1358.
2. Sax, K., The effect of ionizing radiation on plant growth. *American Journal of Botany* **1954,** 42, (4), 360-364.
3. Johnson, E. L., Susceptibility of seventy species of flowering plants to X radiation. *Plant Physiology* **1936,** 11, 319-342.
4. Kersten, H. J.; Miller, H. L.; Smith, G. F., Stimulative effects of X rays on plants. *Plant Physiology* **1943,** 18, 8-18.
5. Borges, H. L.; Linden, R., Gamma irradiation leads to two waves of apoptosis in distinct cell populations of the retina of newborn rats. *Journal of Cell Science* **1999,** 112, 4315-4324.
6. Fricker, S. P., Medical uses of gold compounds: past, present, and future. *Gold Bulletin* **1996,** 29, (2), 53-60.
7. Sun, R. W.-Y.; Che, C.-M., The anti-cancer properties of gold(III) compounds with dianionic porphyrin and tetradentate ligands. *Coordination Chemistry Reviews* **2009,** 253, 1682-1691.
8. Petering, H. G.; Buskirk, H. H.; Underwood, G. E., Antitumor action of 2-oxo-3-ethoxybutyraldehyde bis(thiosemicarbazone) and similar compounds. *Cancer Research* **1964,** 24, 367-372.
9. Parish, R. V.; Cottrill, S. M., Medicinal gold compounds. *Gold Bulletin* **1987,** 20, (1 & 2), 3.
10. Sannella, A. R.; Casini, A.; Gabbiani, C.; Messori, L.; Bilia, A. R.; Vincieri, F. F.; Majori, G.; Severini, C., New uses for old drugs. Auranofin, a clinically established antiarthritic metallodrug, exhibits potent antimalarial effects in vitro: mechanistic and pharmacological implications. *Federation of European Biochemical Societies (FEBS) Letters* **2008,** 582, 844-847.
11. WHO Drug resistance: malaria, http://www.who.int/drugresistance/malaria/en/. (Jun 1, 2010),
12. Eustis, S.; El-Sayed, M. A., Why gold nanoparticles are more precious than pretty gold: Noble metal surface plasmon resonance and its enhancement of the radiative and nonradiative properties of nanocrystals of different shapes. *Chemical Society Reviews* **2005,** 35, 209-217.
13. GE Healthcare, AuroProbe, http://www.gelifesciences.com. (May 28, 2010),
14. Salata, O. V., Applications of nanoparticles in biology and medicine. *Journal of Nanobiotechnology* **2004,** 2, (3).
15. Nripen Chanda, P. K., Lisa D Watkinson, Ravi Shukla, Ajit Zambre, Terry L Carmack, Hendrik Engelbrecht, John R Lever, Kavita Katti, Genevieve M Fent, Stan W Casteel, C. Jeffrey Smith, William H Miller, Silvia S Jurisson, Evan Boote, J David Robertson, Cathy S Cutler, Marina Dobrovolskaia, Raghuraman Kannan, Kattesh V Katti, Radioactive gold nanoparticles in cancer therapy: therapeutic efficacy studies of GA-198AuNP nanoconstruct in prostate tumor-bearing mice. *Nanomedicine: Nanotechnology, Biology, and Medicine* **2009,** 6, (2), 201-209.
16. Williams, M. L., Core chemistry of gold and its complexes. *Inflammopharmacology* **2008,** 16, 110-111.

17. Kautz, H. D.; Storey, R. H.; Zimmerman, A. J., Radioactive drugs. *The American Journal of Nursing* **1964,** 64, (1), 124-128.
18. Turner, A. R.; Gummerman, L. W.; Boggs, D. R., Suppression of hepatic hematopoiesis with radioactive gold (198Au). *The Journal of Nuclear Medicine* **1985,** 26, (4), 366-367.
19. Emery, J. F.; Leddicotte, G. W., *The Radiochemistry of Gold*. National Academy of Science: Oak Ridge National Lab, 1961; p 34.
20. Green, M. A.; Mathias, C. J.; Welch, M. J.; McGuire, A. H.; Perry, D.; Fernandez-Rubio, F.; Perimutter, J. S.; Raichle, M. E.; Bergmann, S. R., Copper-62-labeled pyruvaldehyde bis(N4-methylthiosemicarbazonato)copper(II): synthesis and evaluation as a positron emission tomography tracer for cerebral and myocardial perfusion. *Journal of Nuclear Medicine* **1990,** 31, 1989-1996.
21. Sheldrick, G. M. *SHELXS-97, Crystal structure solution*, University of Gottingen: Gottingen, Germany, 1997.
22. Sheldrick, G. M. *SHELXL-97, Crystal structure refinement*, University of Gottingen: Gottingen, Germany, 1997.
23. Sheldrick, G. M. *SADABS Version 2.10*, University of Gottingen: Gottingen, Germany, 2003.
24. Ortner, K.; Abram, U., Reactions of dichloro[2-(dimethylaminomethyl)phenyl-C^1,*N*]gold(III), [Au(damp-C^1,*N*)Cl2], with aromatic thiosemicarbazones. Structures and spectroscopical data of the first gold(III) thiosemicarbazone complexes. *Inorganic Chemistry Communications* **1998,** 1, (7), 251-253.
25. Abram, U.; Ortner, K.; Gust, R.; Sommer, K., Gold complexes with thiosemicarbazones: reactions of bi- and tridentate thiosemicarbazones with dichloro[2-(dimethylaminomethyl)phenyl-C1,N]gold(III), [Au(damp-C 1,N)Cl2]. *Dalton* **2000**, (5), 735-744.
26. Santos Isabel, G.; Hagenbach, A.; Abram, U., Stable gold(III) complexes with thiosemicarbazone derivatives. *Dalton transactions (Cambridge, England : 2003)* **2004**, (4), 677-682.
27. Sreekanth, A.; Fun, H.-K.; Kurup, M. R. P., Formation of first gold(III) complex of an N(4)-disubstituted thiosemicarbazone derived from 2-benzoylpyridine: structural and spectral studies. *Inorganic Chemistry Communications* **2004,** 7, (12), 1250-1253.
28. Casas, J. S.; Castano, M. V.; Cifuentes, M. C.; Garcia-Monteagudo, J. C.; Sanchez, A.; Sordo, J.; Abram, U., Complexes of dichloro[2-(dimethylamniomethyl)phenyl-C^1,*N*]gold(III), [Au(damp-C^1,*N*)Cl_2], with formylferrocene thiosemicarbazones: synthesis, structure and cytotoxicity. *Journal of Inorganic Biochemistry* **2004,** 98, 1009-1016.
29. Bottenus, B. N.; Kan, P.; Jenkins, T.; Ballard, B.; Rold, T. L.; Barnes, C.; Cutler, C.; Hoffman, T. J.; Green, M. A.; Jurisson, S. S., Gold(III) bis-thiosemicarbazonato complexes: synthesis, characterization, radiochemistry and X-ray crystal structure analysis. *Nuclear Medicine and Biology* **2010,** 37, 41-49.
30. Cowley, A. R.; Davis, J.; Dilworth, J. R.; Donnelly, P. S.; Dobson, R.; Nightingale, A.; Peach, J. M.; Shore, B.; Kerr, D.; Seymour, L., Fluorescence studies of the intra-cellular distribution of zinc bis(thiosemicarbazone) complexes in human cancer cells. *Chemical Communications* **2005**, 845-847.

31. Green, M. A.; Mathias, C. J.; Welch, M. J.; McGuire, A. H.; Perry, D.; Fernandez-Rubio, F.; Perlmutter, J. S.; Raichle, M. E.; Bergmann, S. R., Copper-62-labeled pyruvaldehyde bis(N4-methylthiosemicarbazonato)copper(II): synthesis and evaluation as a positron emission tomography tracer for cerebral and myocardial perfusion. *Journal of Nuclear Medicine* **1990,** 31, (12), 1989-96.
32. Christlieb, M.; Cowley, A. R.; Dilworth, J. R.; Donnelly, P. S.; Paterson, B. M.; Struthers, H. S. R.; White, J. M., New bimetallic compounds based on the bis(thiosemicarbazonato) motif. *Dalton Transactions* **2007**, (3), 327-331.
33. Garcia, M.; Jemal, A.; Ward, E. M.; Center, M. M.; Hao, Y.; Siegel, R. L.; Thun, M. J. *Global Cancer Facts & Figures 2007*; American Cancer Society: Atlanta, GA, 2007.
34. Sahoo, S. K.; Labhasetwar, V., Nanotech approaches to drug delivery and imaging *Drug Discovery Today* **2003,** 8, 1112-1120.
35. Eustis, S.; El-Sayed, M. A., Why gold nanoparticles are more precious than pretty gold: Noble metal
surface plasmon resonance and its enhancement of the radiative and
nonradiative properties of nanocrystals of different shapes. *Chemical Society Reviews* **2005,** 35, 209-217.
36. Buffat, P.; Borel, J.-P., Size effect on the melting temperature of gold particles. *Physical Review A* **1976,** 13, (6), 2287-2298.
37. Castro, T.; Reifenberger, R.; Choi, E.; Andres, R. P., Size-dependent melting temperature of individual nanometer-sized metallic clusters. *Physical Review B* **1990,** 42, (13), 8548-8556.
38. Jadzinsky, P. D.; Calero, G.; Ackerson, C. J.; Bushnell, D. A.; Kornberg, R. D., Structure of a Thiol Monolayer-Protected Gold Nanoparticle at 1.1 A Resolution. *Science* **2007,** 318, (5849), 430-433.
39. Yeh, H. C.; Ho, Y. P.; Wang, T. H., Quantum dot - mediated biosensing assays for specific nucleic acid detection. *Nanomedicine* **2005,** 1, 115-121.
40. Rawat, M.; Singh, D.; Saraf, S., Nanocarriers: promising vehicle for bioactive drugs. *Biological & Pharmaceutical Bulletin* **2006,** 29, 1790-1798.
41. Dong, S.; Roman, M., Fluorescently labeled cellulose nanocrystals for bioimaging applications. *Journal of the American Chemical Society* **2007,** 129, 13810-13811.
42. Skrabalak, S. E.; Au, L.; Lu, X.; Li, X.; Xia, Y., Gold nanocages for cancer detection and treatment. *Nanomedicine* **2007,** 2, 657-668.
43. Cho, K.; Wang, X.; Nie, S.; Chen, Z.; Shin, D. M., Therapeutic Nanoparticles for Drug Delivery in Cancer. *Clinical Cancer Research* **2008,** 14, (5), 1310-1316.
44. Naravanan, R.; El-Sayed, M. A., *Chimica Oggi/Chemistry Today* **2007,** 25, 84-86.
45. Ipe, B. I.; Thomas, K. G.; Barazzouk, S.; Hotchandani, S.; Kamat, P. V., Photoinduced charge separation in a fluorophore-gold nanoassembly. *Journal of Physical Chemistry B* **2002,** 106, (1), 18-21.
46. Maier, S. A.; Atwater, H. A., *Journal of Applied Physics* **2005,** 98.
47. Caseri, W., *Macromolecular Rapid Communications* **2000,** 21, 705-722.
48. Al-Rawashdeh, N.; Foss, C. A., *Nanostructured Materials* **1997,** 9, 383-386.
49. Katti, K. V.; Kannan, R.; Katti, K.; Kattumori, V.; Pandrapraganda, R.; Rahing, V.; Cutler, C.; Boote, E. J.; Casteel, S. W.; Smith, C. J.; Robertson, J. D.; Jurisson, S. S.,

Hybrid gold nanoparticles in molecular imaging and radiotherapy. *Czechoslovak Journal of Physics* **2006,** 56, D23-D34.
50. Kolsky, K. L.; Mausner, L. F., Production of no-carrier added 199Au for gold cluster-labelled antibodies. *Applied Radiation and Isotopes* **1993,** 44, (3), 553-560.
51. Amendola, V.; Meneghetti, M., Size evaluation of gold nanoparticles by UV-Vis Spectroscopy. *Journal of Physical Chemistry C* **2009,** 113, 4277-4285.
52. Haiss, W.; Thanh, N. T.; Aveyard, J.; Fernig, D. G., Determination of size and concentration of gold nanoparticles from UV-vis spectra. *Analytical Chemistry* **2007,** 79, (11), 4215-21.
53. Majzik, A.; Patakfalvi, R.; Hornok, V.; Dekany, I., Growing and stability of gold nanoparticles and their functionalization by cysteine. *Gold Bulletin* **2009,** 42, 113-123.
54. Yoshizawa, S.; Horiuchi, T.; Fujiki, H.; Yoshida, T.; Okuda, T.; Sugimura, T., Antitumor promoting activity of (-)-epigallocatechin gallate, the main constituent of "Tanin" green tea. *Phytotherapy Research* **2006,** 1, (1), 44-47.
55. Lee, J. H.; Kishikawa, M.; Kumazoe, M.; Yamada, K.; Tachibana, H., Vitamin A enhances antitumor effect of a green tea polyphenol on melanoma by upregulating the polyphenol sensing molecule 67-kDa laminin receptor. *PLoS ONE* **2010,** 5, (6), e11051. doi:10.1371/journal.pone.0011051.
56. Ciardiello, F.; Caputo, R.; Bianco, R.; Damiano, V.; Pomatico, G.; Placido, S. D.; Bianco, A. R.; Tortora, G., Antitumor effect and potentiation of cytotoxic drugs activity in human cancer cells by ZD-1839 (Iressa), an epidermal growth factor receptor-selective tyrosine kinase inhibitor. *Clinical Cancer Research* **2000,** 6, 2053-2063.
57. Markowitz, S.; Wang, J.; Myeroff, L.; Parsons, R.; Sun, L.; Lutterbaugh, J.; Fan, R. S.; Zborowska, E.; Kinzler, K. W.; Vogelstein, B., Inactivation of the type II TGF-beta receptor in colon cancer cells with microsatellite instability. *Science* **1995,** 268, (5215), 1336-1338.
58. Lynch, T. J.; Bell, D. W.; Sordella, R.; Gurubhagavatula, S.; Okimoto, R. A.; Brannigan, B. W.; Harris, P. L.; Haserlat, S. M.; Supko, J. G.; Haluska, F. G.; Louis, D. N.; Christiani, D. C.; Settleman, J.; Haber, D. A., Activating mutations in the epidermal growth factor receptor underlying responsiveness of non-small-cell lung cancer to gefitinib. *The New England Journal of Medicine* **2004,** 350, (21), 2129-2139.
59. Hynes, N. E.; Lane, H. A., ERBB receptors and cancer: the complexity of targeted inhibitors. *Nature Reviews Cancer* **2005,** 5, 341-354.
60. Mendelsohn, J., Targeting the epidermal growth factor receptor for cancer therapy. *Journal of Clinical Oncology* **2002,** 20, (18), 1s-13s.
61. Reubi, J. C.; Waser, B.; Schaer, J. C.; Laissue, J. A., Somatostatin receptor sst1-sst5 expression in normal and neoplastic human tissues using receptor autoradiography with subtype-selective ligands. *European Journal of Nuclear Medicine* **2001,** 28, (7), 836-846.
62. Herder, W. W. d.; Hofland, L. J.; Lely, A. J. v. d.; Lamberts, S. W. J., Somatostatin receptors in gastroenteropancreatic neuroendocrine tumours. *Endocrine-Related Cancer* **2003,** 10, 451-458.
63. Zhang, X.; Cai, W.; Cao, F.; Schreibmann, E.; Wu, Y.; Wu, J. C.; Xing, L.; Chen, X., 18F-labeled bombesin analogs for targeting GRP receptor-expressing prostate cancer *Journal of Nuclear Medicine* **2006,** 47, (3), 492-501.

64. Fleischmann, A.; Waser, B.; Reubi, J. C., High expression of gastrin-releasing peptide receptor in the vascular bed of urinary tract cancers: promising candidates for vascular targeting applications. *Endocrine-Related Cancer* **2009,** 16, (2), 623-633.
65. Okarvi, S. M.; Al-Jammaz, I., Synthesis, radiolabelling and biological characteristics of a bombesin peptide analog as a tumor imaging agent. *Anticancer Research* **2003,** 23, (3B), 2745-2750.
66. Conrad, D. Tumor-seeking nanoparticles *Periodical* [Online], 2006, p. 1-3.
67. Okarvi, S. M., Recent developments in 99Tcm-labelled peptide based radiopharmaceuticals: an overview. *Nuclear Medicine Communication* **1999,** 20, 1093-1112.
68. Boerman, O. C.; Oyen, W. J. G.; Corstens, F. H. M., Radio-labeled receptor-binding peptides: a new class of radiopharmaceuticals. *Seminars in Nuclear Medicine* **2000,** 30, 195-208.
69. Kattumuri, V. Gold nanoparticles for biomedical applications: synthesis, characterization, in vitro and in vivo studies. University of Missouri, Columbia, MO, 2006.
70. Reile, H.; Armatis, P. E.; Schally, A. V., Characterization of high-affinity receptors for bombesin/gastrin releasing peptides on the human prostate cancer cell lines PC-3 and DU-145: internalization of receptor bound 125I-(Tyr4) bombesin by tumor cells. *Prostate* **1994,** 25, (1), 29-38.
71. Vincentis, G. D.; Scopinaro, F.; Varvarigou, A.; Ussof, W.; Schillaci, O.; Archimandritis, S.; Corleto, V.; Longo, F.; Fave, G. D., Phase I trial of technetium [Leu13] bombesin as cancer seeking agent: possible scintigraphic guide for surgery? *Tumori* **2002,** 88, (3), S28-30.
72. Schuhmacher, J.; Zhang, H.; Doll, J.; Macke, H. R.; Matys, R.; Hauser, H.; Henze, M.; Haberkorn, U.; Eisenhut, M., GRP receptor-targeted PET of a rat pancreas carcinoma xenograft in nude mice with a 68Ga-labeled bombesin(6-14) analog. *Journal of Nuclear Medicine* **2005,** 46, (4), 691-699.
73. Montet, X.; Yuan, H.; Weissleder, R.; Josephs, L., Enzyme-based visualization of receptor-ligand binding in tissues. *Laboratory Investigation* **2006,** 86, 517-525.
74. Sonavane, G.; Tomoda, K.; Makino, K., Biodistribution of colloidal gold nanoparticles after intravenous administration: effect of particle size. *Colloids and Surfaces B: Biointerfaces* **2008,** 66, 274-280.
75. Semmler-Behnke, M.; Kreyling, W. G.; Lipka, J.; Fertsch, S.; Wenk, A.; Takenaka, S.; Schmid, G.; Brandau, W., Biodistribution of 1.4- and 18-nm gold particles in rats. *Small* **2008,** 4, (12), 2108-2111.
76. Kawano, T.; Yamagata, M.; Takahashi, H.; Niidome, Y.; Yamada, S.; Katayama, Y.; Niidome, T., Stabilizing of plasmid DNA in vivo by PEG-modified cationic gold nanoparticles and the gene expression assisted with electrical pulses. . *Journal of Controlled Release* **2006,** 111, 382-389.
77. Niidome, T.; Yamagata, M.; Okamoto, Y.; Akiyama, Y.; Takahashi, H.; Kawano, T.; Katayama, Y.; Niidome, Y., PEG-modified gold nanorods with a stealth character for in vivo applications. *Journal of Controlled Release* **2006,** 114, 343-347.
78. Hoffman, T. J.; Gali, H.; Smith, C. J.; Sieckman, G. L.; Hayes, D. L.; Owen, N. K.; Volkert, W. A., Novel series of 111In-labeled bombesin analogs as potential radiopharmaceuticals for specific targeting of gastrin-releasing peptide receptors

expressed on human prostate cancer cells. *Journal of Nuclear Medicine* **2003,** 44, 823-831.
79. Abram, U.; Ortner, K.; Gust, R.; Sommer, K., Gold complexes with thiosemicarbazones: reactions of bi- and tridentate thiosemicarbazones with dichloro[2-(dimethylaminomethyl)phenyl-C1,N]gold(III), [Au(damp-C 1,N)Cl2]. *Dalton* **2000,** 5, 735-744.
80. Isabel, G. S.; Hagenbach, A.; Abram, U., Stable gold(III) complexes with thiosemicarbazone derivatives. *Dalton Transactions* **2004,** 4, 677-682.
81. Sreekanth, A.; Fun, H. K.; Kurup, M. R. P., Formation of the first gold(III) complex of an N(4)-disubstituted thiosemicarbazone derived from 2-benzoylpyridine: structural and spectral studies *Inorganic Chemistry Communications* **2004,** 7, (12), 1250-1253.
82. Esumi, K.; Houdatsu, H.; Yoshimura, T., Antioxidant action by gold-PAMAN dendrimer nanocomposites. *Langmuir* **2004,** 20, 2536-2538.